TABLE OF CONTENTS

ABSTRACT v

I. INTRODUCTION. 1

II. EXPERIMENTAL PROCEDURE. 5

A. Materials Preparation 5

B. Heat Treatment. 5

1. Intermediate Quenching. 5

2. Continuous Annealing. 6

C. Mechanical Testing. 6

1. Tensile 6

2. Impact. 7

D. Dilatometry 7

E. Metallography 8

1. Optical 8

2. Transmission Electron Microscopy. 8

3. Fractography. 9

F. Volume Fraction Determinations. 9

III. RESULTS AND DISCUSSION. 10

A. Microstructures 11

1. Intermediate Quenching vs. Continuous Annealing (1010) 11

2. Intermediately Quenched 1010 and 1020 14

a. Martensite Morphology 14

b. Additional Microstructural Features 15

c. Tempered Microstructures. 16

NOTICE
This report was prepared as an account of work sponsored by the United States Government. Neither the United States nor the United States Department of Energy, nor any of their employees, nor any of their contractors, subcontractors, or their employees, makes any warranty, express or implied, or assumes any legal liability or responsibility for the accuracy, completeness or usefulness of any information, apparatus, product or process disclosed, or represents that its use would not infringe privately owned rights.

DISTRIBUTION OF THIS DOCUMENT IS UNLIMITED

d. Impact Fracture Surfaces 17

B. Mechanical Properties. 17

1. Tensile. 17

a. Intermediate Quenching vs. Continuous Annealing (1010) 17

b. Intermediately Quenched 1010 and 1020. 18

i. As quenched. 19

ii. Tempered 20

2. Impact 22

a. Intermediately Quenched 1010 And 1020. 22

b. DBTT (1020). 23

C. Mechanical Property/Microstructure Correlations. 24

1. Quantitative (Empirical) Relationships 24

2. Qualitative Relationships. 29

D. Comparison To Commercial Specifications. 31

IV. CONCLUSIONS. 33

ACKNOWLEDGMENTS 35

REFERENCES. 36

TABLES. 39

FIGURE CAPTIONS 43

FIGURES 47

HEAT TREATMENT AND CHARACTERIZATION OF DUPLEX 1010 AND 1020 STEELS

M. J. Young

Materials and Molecular Research Division
Lawrence Berkeley Laboratory
and Department of Materials Science and Engineering
University of California, Berkeley, California 94720

ABSTRACT

An investigation concerning the heat treatment of duplex ferritic-martensitic 1010 and 1020 steels has been carried out. Tensile and impact properties of intermediately quenched and continuously annealed specimens have been characterized and microstructural correlations established. The rule for two phase mixtures may be used as a fairly good approximation of the mechanical behavior of the duplex system, and improved correlations are possible with suitable modifications for the size, shape and distribution of the second phase.

The property differentials between the duplex 1010 and 1020 at equal volume fractions of martensite are due mainly to the higher carbon content (hence, higher strength) of the 1020 martensite. Important metallurgical variables include subgrain formation, retained austenite, transformation twinning and martensite fraction. Of these, the volume fraction of martensite appears to be the most influential in controlling the strength, ductility and impact properties of the duplex systems studied.

ACKNOWLEDGMENTS

I would like to thank Professor Gareth Thomas for suggesting this research program, and for continuous guidance and encouragement. I would also like to thank my many friends, particularly Lorin and Mary Brass, who made the time I spent in Berkeley enjoyable. I would especially like to express my appreciation to my good friend Jayoung Koo, for his invaluable assistance in all phases of this work.

This work was done under the auspices of the U. S. Department of Energy through the Materials and Molecular Research Division of the Lawrence Berkeley Laboratory.

I. INTRODUCTION

The ever increasing emphasis on energy and resource conservation has triggered intensive development programs resulting in the introduction of new steel compositions and processing techniques. Many programs, e.g., weight savings in the transportation industry, have concentrated efforts in the area of high strength, low alloy (HSLA) steels which derive their principal strengthening from finely dispersed Niobium, Vanadium or Titanium carbides. Many design goals have been met with the HSLA steels, although formability appears to be a problem and in numerous cases the alloying and processing economics more than offset cost reductions due to the strength-to-weight increase. Alternative emphasis, both commercially[1] and academically,[2-5] toward duplex, low carbon steels has thus increased, and results have been very promising.

The processing of steels to obtain the microduplex structure of martensite in a dislocated ferrite matrix is not an entirely new concept. The duplex ferritic-martensite aggregates can be obtained in several ways, thus mechanical, thermal-mechanical and thermal methods have been investigated. Cairns and Charles[6] instituted an early program aimed at developing laminates and composites through combinations of mechanical work and heat treatment. They achieved only limited success, especially with commercial steels, but did propose a useful model for the fiber strengthening of steel. A viable alternative utilizes annealing in the two phase field; however the

microduplex structures cannot be formed in every combination of alloy compositions and annealing temperatures. Diffusion characteristics and such phenomena as reverse martensitic transformations prevent that formation in some systems.[7] Duplex processing concepts have been applied to nonferrous as well as ferrous systems, but with considerably more emphasis on the latter. Hwang[8] and Jin et. al.,[9] have utilized the ($\alpha + \gamma$) region in maraging steels to obtain desirable properties in cryogenic applications, and Enomoto and Furubayashi[7] have studied the vast two phase region in iron-nickel alloys. The beneficial effects of refined grain size have been asserted by many researchers, and are well understood and documented. Miller[10] has shown that stable, ultra-fine grained microstructures can be obtained by annealing cold worked alloys at relatively low temperatures in the ($\alpha + \gamma$) range. Similarly, work by Snape and Church[11] with low alloy steels has shown that the presence of the newly formed phase at the grain boundaries of the primary phase can effectively retard grain growth. The combined strength increases from grain refinement and the presence of martensite (which acts as the load carrying constituent), coupled with the ductility inherent in the ferrite matrix has been utilized recently by Koo[4] and Koo and Thomas,[2] using commercial 1010 and experimental alloys. In their work a thermal process originated by Grange[12] was modified to include two phase annealing which significantly increased strength while maintaining good elongation ductility. Industrial research with these duplex alloys[13] has shown that significant strengthening and work hardening can be obtained with thermal-mechanical

treatment. After tempering, the martensite-ferrite aggregate is of intermediate strength with ductility equivalent to HSLA steels of comparable strength.

Thus, the advantages of duplex microstructures have been established in several alloy systems. Applications to the low carbon steels are especially interesting for several reasons: (1) compositions and required heat treatments are basically simple, with the possibility of eliminating the need for thermal-mechanical processing, (2) a very high tonnages are used commercially and (3) considerable scope for increasing strength while maintaining good ductility appears possible. This has been a driving force for the ongoing duplex steel design program in Professor Thomas' group. It is aimed at characterizing the duplex microstructure/mechanical property relations with particular emphasis on further improvements in mechanical properties, and a fundamental understanding of their origins. As part of this design program, the present research was intended to establish structure-property relationships in high purity 1010 and 1020 steels (0.1 and 0.2 weight percent carbon, respectively) and precedes selected ternary and quaternary additions to the base alloy. The immediate research objectives were:

(1) Determine the effects of carbon, in the separate phases as well as in the overall composition.

(2) Characterize the duplex microstructure in terms of martensite and ferrite quantities, and establish the microstructure-property relations.

(3) Determine if further mechanical property improvements, solely be heat treatment, would be possible.

Results of the previous work by Koo[3,4] have been utilized; specifically, that cycling in the $(\alpha + \gamma)$ region more than once does not result in further grain refinement nor substantial improvement in mechanical properties. Investigations concerning processing to obtain the duplex microstructure, tempering effects and impact behavior also have been completed.

II. EXPERIMENTAL PROCEDURE

A. MATERIALS PREPARATION

High purity 1010 and 1020 alloys of the composition shown in Table 1 were vacuum arc remelted and cast as 20 pound ingots. These ingots were subsequently upset forged to approximately 0.5 in. thickness. Portions were further reduced to approximately 0.15 in. by cold rolling.

B. HEAT TREATMENT

1. Intermediate Quenching.

Oversize flat tensile and Charpy impact specimens were austenitized in a vertical tube furnace (resistance heating) under an argon atmosphere for 30 minutes at 1100 °C, and quenched directly into agitated iced brine. Microhardness measurements were taken across numerous cross sections and compared to values obtained by other researchers.[14,15,16] Later transmission electron microscopy showed the structures to be almost fully martensitic and free of undissolved carbides. Further thermal treatments were accomplished according to the following schedule:

a. Two Phase Annealing.

Oversize tensile and Charpy specimens were reheated to the desired temperature in the ($\alpha + \gamma$) field and held for 20 minutes. The vertical furnace with protective argon atmosphere was again used. The specimens were then quenched directly into iced brine. Extensive

optical metallography revealed almost no evidence of texture resulting from the forging or cold rolling operations.

b. Tempering.

Tempering of the martensitic and duplex alloys was effected by immersing the samples in a neutral salt bath at 200 °C for 30 minutes. Selected samples were also tempered at 400 °C and 600 °C for 30 minutes.

2. Continuous Annealing.

Oversize flat tensile specimens of the 1010 alloy were encapsulated in quartz tubes which were then evacuated and backfilled with 20 inches of argon. These were austenitized in a box furnace at 1100 °C for 30 minutes and then transferred directly to an adjacent furnace at the desired two phase temperature and held for 20 minutes. The specimens were then directly quenched into agitated iced brine; the quartz capsules were imploded simultaneously with immersion in the iced brine to ensure rapid quenching.

C. MECHANICAL TESTING

1. Tensile.

Tensile properties were determined using the flat tensile specimens shown in Figure 2A. The specimens were originally machined oversize, heat treated and ground to final dimensions. Approximately 0.025 in. was removed from each side to eliminate the possible effects of surface decarburization. Optical metallography revelaed decarburization did not exceed approximately 10 mils.

Tensile tests were performed at room temperature on a calibrated Instron machine using a cross head speed of 0.05 cm/min and full scale load of 1000 Kg. Uniform elongation was continuously monitored with an optical magnifier accurate to 0.001 in. Total elongation was determined by measuring gage lengths before and after testing with an optical microscope equipped with a vernier translating stage accurate to 0.001 in.

2. Impact.

Impact properties were determined using the standard and subsize Charpy V-notch specimens shown in Figure 2B. The low hardenablity of the 1010 alloy precluded the use of fullsize specimens, and subsize 1020 specimens were included for comparison. Impact tests were performed using a Universal Impact machine with calibrated units of 0.25 ft. lbs. Low and high temperature testing was conducted according to ASTM specifications.[17] Zero and sub-zero temperatures were controlled using mixtures of ethyl alcohol and dry ice.

D. DILATOMETRY

Dilatometric methods were used to determine the austenite start, A_s, and austenite finish, A_f, temperatures as a prelude to determining the A_3 and A_1 temperatures for the 1010 and 1020 steels. Martensitic transformation temperatures, M_s and M_f, for the completely martensitic and duplex alloys also were determined.

E. METALLOGRAPHY

1. Optical.

Sections to be used for optical metallography were cut from fractured tensile and impact specimens and mounted in Koldmount, Bakelite or Lucite. The specimens were mechanically ground to 600 grit, ultrasonically cleaned and polished on a 1 micron rotating diamond abrasive wheel lubricated with kerosene. The standard etchants 2% Nital, 5% Nital and Kallings reagent were used to reveal the ferritic and martensitic structures. Prior austenite grain boundaries were revealed by immersion in an etch solution of 1 g picric acid, 1 g dodecylbenzene sulfonate and 100 ml of water. Samples were examined on the Zeiss Ultraphot II metallograph equipped with a Nomarsky interference contrast apparatus.

2. Transmission Electron Microscopy.

Specimens of approximately 0.150 in. thickness for thin foils were treated with the tensile and impact specimens, and carefully ground to 30 mils. Approximately equal amounts were removed from each side while utilizing flood cooling to minimize specimen heating. The specimens were then chemically thinned to less than 10 mils in a solution of H_2O_2 containing 2% HF at room temperature. 3.0 mm discs were spark cut and mechanically sanded to 1-2 mils, cleaned with acetone and electropolished in a twin jet polishing apparatus at room temperature using a chromic-acetic solution

(75 g CrO_3 + 400 ml CH_2COOH + 21 ml distilled H_2O). Polishing times varied from 3 to 5 minutes at 30-35 ma and 25-30 volts. Foils were examined in a JEM 7A electron microscope at an accelerating voltage of 100 KV.

3. Fractography.

Fracture surfaces of tensile and impact specimens were examined using an AMR 1000 scanning electron microscope with secondary emission at 25 KV. Specimens were cut, ultrasonically cleaned and stored in dessicators until examination.

F. VOLUME FRACTION DETERMINATIONS

Two methods were used in the martensite fraction measurements: the linear intercept method, and the systematic count method[18] using a scribed eyepiece. Measurements were made on many optical micographs and fields of view, on Charpy and tensile fractures and at various magnifications. Values using the two methods were averaged and rounded to the nearest 5%.

III. RESULTS AND DISCUSSION

Heat treatment in the two phase field does not necessarily involve equilibrium conditions, and the temperatures, the line (lever rule) and composition determinations as specified by the equilibrium diagram[19] are not necessarily applicable. The determination of the A_1, (eutectoid) and A_3 (γ solidus) temperatures for the exact composition was thus necessitated, and extensive experimental heat treatments near the A_s and A_f temperatures (from dilatometry) were conducted. Based on optical metallography, the A_3 temperatures were determined to be ~855 °C for 1010 and ~815 °C for 1020. The A_1, for both alloys was ~710 °C. The amount of phase separation corresponding to 20 minutes at the holding temperature was determined in the same manner.

Qualitatively, the lower limit of the acceptable range of martensite volume fractions (V_m) is restricted to the value where no strengthening of the duplex alloy occurs. The upper limit is set when the failure of the martensite immediately leads to the failure of the duplex structure, i.e., ferrite is not present in sufficient quantity to contribute to toughness and ductility. Of course, the final range of V_m will be determined from specifications and applications for which the steel will be used. Important parameters may include strength, ductility, impact resistance (toughness), formability, weldability, etc.

One of the more important (and difficult to arcumvent) results of the non-equilibrium conditions concerns the composition of the martensite in the duplex structure. The low atomic weight of carbon prevented its chemical analysis by x-ray spectroscopic means, e.g., the EDAX attachment of the SEM. Diamond pyramid microhardness measurements of the martensite in the continuously annealed material appeared to show a valid correspondence (nonlinear) to the volume fraction, which is inversely proportional to carbon content at a given temperature. The fineness of the structure of the intermediately quenched material prohibited valid testing: indentations resulted in the deformation of the surrounding ferrite. The microhardness/volume fraction relationship will be discussed in a later section. One equilibrium relationship is that at equal volume fractions, i.e., different tie lines, the martensite in the 1020 will have a higher carbon content than the martensite in the 1010 (see Figure 1). As will be shown, experimental evidence supports the validity of this relationship for the duplex system.

A. MICROSTRUCTURES (OPTICAL, TEM, FRACTOGRAPHY)

1. Intermediate Quenching vs. Continuous Annealing (1010).

The initial microstructure is important in the duplex processing of steel, and martensite has been shown to be favorable because of the numerous fine heterogeneities in the structure.[2,4] Figure 3A shows the martensitic structure of the steels before being

subjected to the duplex treatments of Figure 1. In the intermediate quenching process, reheating to the two phase temperature after quenching from austenite results in the nucleation of austenite at prior austenite grain boundaries, martensite lath boundaries, dislocations and other quenched-in imperfections. The high density of nucleation sites coupled with the slower reaction rate results in a fine dispersion of martensite 'islands' in the ferrite matrix as shown in Figure 3, B and D.

In the continuous annealing process (Figure 1C), the structure prior to two phase annealing is austenite. Decreasing the temperature to the two phase region results in several changes necessary for the nucleation of ferrite: there is a fluctuation in carbon content and a local change in crystal structure.[23] The ferrite nucleates at the prior austenite grain boundaries because the surface energy barrier is reduced,[23-25] and grows into the austenite matrix. The microstructure thus depends upon prior austenite grain size and tends to be coarser than that obtained from martensite as shown in Figure 3C.

The nucleation and kinetic differences in the two processes were most evident in micrographs with increasing percentages of martensite. In the intermediately quenched material, the existing martensite islands did not grow appreciably, but more austenite (martensite after quenching) nucleated. In the continuously annealed specimens, the number of nucleation sites did not appear to change, and the martensite regions grow significantly.

Several striking differences in the microstructural aspects of the two processes were evident in TEM examination. The ferrite regions in all the specimens were locally heavily dislocated as a result of accommodating the martensite transformation strain, but the significant difference in proeutectoid morphologies was subgrain size. The ferrite grains in the continuously annealed specimens were very large, and there was no observable division into subgrains. The proeutectoid ferrite in the intermediately quenched material had a network of subgrains spaced an average of 0.5 to 1 micron apart. The ferrite region in this process does not undergo a phase transformation as the alpha (martensite) is annealed in the two phase region. As a result, the dislocations generated by the martensitic transformation (on quenching from 1100 °C) rearrange themselves into dislocation walls and form subboundaries in the proeutectoid constituent during the two phase annealing. Figures 4 and 5 illustrate the subgrain formation, which is regarded as an important strengthening mechanism. Warrington[26] reported that subgrain size can be related to the flow stress of iron by the Hall-Petch equation.

In the continuously annealed material almost all martensite/ferrite interfaces were microscopically regular and smooth. While smooth interfaces were evident in the intermediately quenched specimens, martensite laths (Figure 4) and regularly shaped regions (Figure 5A) were very prevalent. The ferrite in the immediate vicinity of martensite/ferrite interfaces showed numerous regions of fibrous carbide precipitation resembling pearlite as shown in Figure 6.

As is evident from the figure, such carbides were present from both processes. The carbides presumably remain after the moving ferrite/austenite boundary grew into the matrix after the nucleation of the $\gamma \rightarrow \alpha$ + carbide reaction. There appeared to be a higher and more localized density of the fibrous carbides in the continuously annealed specimens. Positive identification of the carbides was not possible because of the complexity of the diffraction patterns from such areas. The morphology of such carbides is similar to that observed in simple chromium steels by Campbell and Honeycombe[27] who identified the carbides as M_7C_3, produced by pearlitic type of reaction.

Scanning electron fractographs of the tensile failures for the two processes are shown in Figures 7 and 8. Figure 7A shows the the predominantly dimpled rupture surface of sample 1B which is indicative of a completely ductile failure. Figure 8 shows the fracture surfaces of the continuously annealed materials at various magnifications. Evidence of ductile failure is apparent, but areas of cleavage failure are equally evident in A and B. High magnification views of separate areas (C and D) emphasize the two failure modes. Reduction in area measurements were not made, but the continuously annealed material failed after considerably less necking than the intermediately quenched specimens.

2. <u>Intermediately Quenched 1010 And 1020</u>.

a. Morphology of Martensite.

The characteristic features of the martensite in the 1010 and 1020 steels after directly quenching from 1100 °C can be seen in

Figures 9 and 10. The microstructure consisted almost entirely of laths 0.1 to 0.3 microns wide. Krauss and Marder[28] suggest that each lath forms directly from an independent, homogeneous shear, and successive shears produce a packet. The broad faces of the laths were often visible, thereby allowing the packet boundaries to be delineated, as in Figure 9A. The lath boundaries are frequently of low angle character, whereas the packet boundaries are usually high angle.[29,30] The morphology of martensite in duplex specimens did not differ significantly from the fully martensitic specimens. Figure 9C shows the complex intersection of laths in specimen 1B, and Figure 4 shows a martensite region embedded in the ferrite in specimen 2B.

Another prominent feature of the martensite was the occurrence of autotempering. The autotempered carbides were of the highest density in the completely martensitic structures but were evident in the ferrite of duplex alloys also. The carbide diffraction spots were very weak, so the carbides were tentatively identified by trace analysis. Most of the carbides were cementite in the typical {110} Widmanstatten orientation shown in Figure 10. The carbide morphology was not observed to vary with V_m.

b. Additional Microstructural Features.

The observation of retained austenite was not unexpected since its presence in such low carbon steels had been detected earlier by Koo.[2,31] The extremely thin films of remained austenite that were trapped between growing martensite laths were identified by indexing selected area diffraction patterns such as the one given in Figure 11C.

Figure 11A is the bright field and Figure 11B is the dark field where the retained austenite reversed contrast when the $(002)_\gamma$ reflection was imaged. Figure 11D shows the indexed pattern which proves the martensite and austenite exhibit the Kurdjumov-Sachs orientation relationships, $\langle 111 \rangle_\alpha \parallel \langle 110 \rangle_\gamma$.

Very fine internal twins such as shown in Figure 12 were observed in all of the duplex specimens, and are indicative of localized carbon enrichment. While no intentional effort to establish the amount of twinning was made, the twinning was more evident at lower martensite fractions and in the 1020 foils.

The descriptions of ferrite and carbide morphologies for the intermediately quenched 1010 apply also to the intermediately quenched 1020 steel. As is evident from Figure 7, the fracture surfaces for the two intermediately quenched alloys were also very similar.

C. TEMPERED MICROSTRUCTURES

Tempering at 200 °C is of considerable practical interest because the steel sheet is very likely to encounter such conditions during processing, e.g., galvanizing, painting, etc. Tempering of the 1010 and 1020 at 400 and 600 °C is of comparatively less practical importance and was carried out mainly to investigate the property trends. An effort to investigate the microstructural aspects after tempering was thus not attempted. A detailed microstructural analysis of tempering of the duplex structure is forthcoming.[32]

d. Impact Fracture Surfaces.

The fracture surfaces of the duplex alloys were very interesting because at most temperatures they showed localized dual modes of failure. Ductile failure, as evident by dimpled rupture, and the characteristic river patterns of cleavage are apparent in Figures 13 and 14; most failures could then be characterized by quasicleavage. There was some isolated evidence of secondary cracking, as in Figure 14C. An analysis to determine unambiguously the origin of such areas as in Figure 13A, e.g., by polishing and etching a plane normal to the fracture surface, is in progress.[32]

B. MECHANICAL PROPERTIES

1. Tensile.

a. Intermediate Quenching vs. Continuous Annealing (1010).

A comparison of mechanical properties for the two treatments is aided by examination of Figure 15. A striking observation is that the strengths of the continuously annealed material appear to be very insensitive to changes in the martensite percentage. This may be considered more unusual because the elongations are equally as sensitive as those for intermediate quenching. Below approximately 40% martensite the strengths for continuous annealing are superior to those for intermediate quenching. Examination of the optical micrographs (Figure 3) assists in the explanation. Maintaining equal volume fractions, at low values of V_m the martensite in the intermediately quenched materials is very uniformly and finely dispersed.

The martensite in the continuously annealed specimens is uniformly dispersed also, but the much larger regions are more interconnected and thus carry more of the load than the intermediately quenched martensite. This advantage can be seen to be decreasing as V_m increases, and past ~40% the strength of the intermediately quenched material is greater, presumably due to the finer martensite dispersion and strengthening of ferrite due to subgrain formation. As mentioned previously, the elongation values for the continuously annealed specimens are sensitive to V_m. Uniform elongations are 2% lower and total elongations are 4% lower than for intermediate quenching, and the variance changes little over the range of V_m tested.

b. Intermediately Quenched 1010 And 1020.

A comparison of the duplex 1010 and 1020 alloys is especially interesting because the effects of carbon in the separate phases, as well as in the total alloy content, may be very pronounced. The prior austenite grain sizes of the duplex steels were compared to the standard ASTM charts and determined to be ASTM #5 (7 to 8 microns) for all duplex treatments. Therefore, this grain size, one of the most important factors in controlling the strength and associated ductility of low carbon steels,[16] may be eliminated as a variable.

The 1010 and 1020 steels were subjected to the two phase annealing processes shown in Figure 1, A and B. Admittedly, the holding time of 20 minutes in the two phase region does not result in the phase separation dictated by the equilibrium diagram, but because the holding time was constant, any deviations from equilibrium are

expected to be relatively small. For a given alloy, the two phase temperatures used to obtain differing volume fractions of martensite were sufficently close, e.g., 15-20 °C, that no marked kinetic differences would be expected. One relationship evident from equilibrium, as discussed previously, is that at equal volume fractions the martensite in the duplex 1020 steel has a higher carbon percentage than the martensite in the 1010. Carbon content is the most important factor in determining martensite strength, as has been documented by many researchers.[14-16]

i. As Quenched

When the duplex specimen is subjected to standard tensile testing, there are two stress regions of concern. From the beginning of the test and until the yield stress is reached, the primary deformation occurs in the ferrite because it is the continuous phase. It can then be seen that for a given V_m and morphology that the strength of the martensite does not play an important role in determining the yield strength. The carbon contents of the ferrite in the 1010 and 1020 are essentially equal, so there should be little difference in the yield strengths of the two steels. As Figure 16 shows, the yield strengths of the 1010 and 1020 differ by a maximum of ~5 ksi. Given the limited accuracy of the volume fraction and strength determinations, it can be seen that the yield strengths are very nearly equal, in agreement with the previously mentioned considerations of continuum mechanics.

The deformation of the martensite is initiated shortly after plastic flow begins and is accelerated at the onset of localized deformation (necking). The larger differences in the ultimate strengths of the two alloys reflect the differences in martensite strength due to carbon enrichment. The difference increases noticeably as the volume fraction increases because there is less ferrite present and the differences in the strengths of the carbon enriched martensites are accentuated. As of course are the differences in work hardening.

The preceding arguments may be used to explain the elongation results also. Uniform elongation is measured until necking occurs, and mainly reflects the deformation of the ferrite. As can be seen from Figure 16, the uniform elongations are nearly equal (0.5% maximum differences). Total elongation encompasses the entire stress region of martensite deformation, and the larger differences between the 1010 and 1020 are again reflective of the martensite strength (and ductility) differences.

As expected, the common relationship of decreasing ductility with increasing strength is observed for both alloys.

ii. Tempered

The tensile properties of the two steels after tempering at 200 °C are shown as functions of the fraction of martensite in Figure 17. The relative positions of the yield curves are reversed from the untempered condition; a situation not to be expected. This is possibly an indication of the tolerances in tensile values and martensite volume determinations. The small fluctutation in martensite

percentage from sample to sample (as evidenced optically) is included in the latter uncertainty.

The properties of the fully martensitic materials did not change appreciably on tempering at 200 °C, mainly attributable to the high density of autotempering (quench tempering). The ultimate strengths of the fully martensitic structures increase slightly after tempering, presumably due to disperison hardening offset (not quite equally) by a depletion of carbon in solid solution. Small increases may also be attributed to increased carbond segregation to, and locking of, dislocations.[22]

The duplex steels had significant strength decreases after 200 °C tempering, as shown in Figure 18. Carbide precipitation did not occur in the ferrite during quenching presumably because there was unsufficient time for carbon to diffuse over the large distances involved. During the 30 minutes at 200 °C carbon had sufficient time to diffuse into the depleted ferrite regions leading to carbide precipitation.

The yield and ultimate strengths of the duplex alloys appear to have an equal sensitivity to tempering at 200 °C, and strength/elongation ductility relationships (Figure 23) appear to be changed from the as quenched condition.

The strengths of the 1010 and 1020 steels containing 35 and 40% martensite, respectively, in the as quenched and tempered conditions are shown in Figure 18. The alloys respond similarly to tempering at 200, 400 and 600 °C. As expected, the ultimate strengths

are more sensitive than the yield strengths. The elongation curves show that the ductility (especially as evidenced by the total elongation) of the 1020 is more influenced than that of the 1010, and the ductility in general is influenced more by tempering than is the strength.

2. Impact.

a. Intermediately Quenched 1010 and 1020.

As previously mentioned, the low hardenability of the 1010 prohibited the use of full size charpy impact specimens. Preliminary tests established that the maximum thickness that could be quenched to a fully martensitic structure was approximately 190 mils, so the subsize specimens shown in Figure 2 were used. Standard size specimens were used for the 1020 steel, and subsize were also included for comparison.

In low carbon steels, increasing the Pearlite content increases the strain hardening rate[33] and decreases the radius of an advancing fibrous crack[21] in materials containing fractions of the hard second phase. This increases the degree of stress intensification ahead of advancing tear and facilitates cleavage.[21] The situation in the duplex structure may be analogous. The hard, second phase martensite increases the stress intensification and decreases the amount of energy absorbed, as is clearly shown in Figure 19. The increase in martensite volume fraction from 25 to 50% decreases the impact energy (especially in the full-size 1020), presumably due to the aforementioned reasons. The increasing cleavage as V_m increases was also evident in

the SEM study of the fractured specimens.

There is some variance in curve shape from 1010 and 1020, and fullsize to subsize, but an essentially similar behavior is suggested. Comparing the magnitudes of subsize full-size is incorrect, because the failure mode is surely affected by specimen geometry. The different slopes of the 1020 subsize vs. fullsize curves may be indicative of this. Concerning subsize specimens though, 1010 specimens showed a quite pronounced shear lip at all martensite fractions while the 1020 did only for the fully martensitic structure. The difference in impact energy is evident from Figure 19, and an obvious conclusion is that at equal volume fractions (but different strengths) 1010 is more resistant to crack initiation (which the charpy test is indicative of) than is the 1020.

In all cases, the fully martensitic structures show higher impact values than any of the duplex structures, presumably due to the effects of the second phase in stress intensification. Predicting behavior from 50 to 100% martensite may be considered purely speculative, as it would be below 25%. Impact values for a completely ferritic structure, while having practical significance, would be useful in showing the relationship here. Isolated tests indicate that the impact energies absorbed by the completely ferritic structure exceed those of the martensitic structure.

b. DBTT (1020).

Fullsize 1020 specimens were tested from -75 to +90 °C to determine the ductile-brittle transition temperature (DBTT) for the

fully martensitic and duplex steels. As is evident from Figure 20 there is no sharp transitions; approximately 150 °C separates the upper and lower shelf energies. Using the average energy criterion, the DBTT would be approximately 25 °C; room temperature impact values are about 1/2 of the upper shelf energy. An important observation is that no significant change in the shape of the DBTT curves occurs as V_m varies. SEM observations of the surfaces fractured at 90 °C revealed that the fully martensitic structure failed in a completely ductile manner, while the duplex alloys showed some evidence of cleavage. This indicates some change in DBTT from the fully martensitic to the duplex alloys, but the difference is small. Of interest also is that at 90 °C the values for 25% martensite are very close to the 100% martensite values with the consideration that some cleavage was still apparent in A, the true upper shelf values are expected to be approximately equal.

C. MECHANICAL PROPERTY/MICROSTRUCTURE CORRELATIONS

1. Quantitative (Empirical) Relationships.

An initial objective of this research was to determine if the behavior of the duplex alloys could be approximated by the well known rule for two phase mixtures:

$$S_c = S_m V_m + S_f(1 - V_m) \qquad (1)$$

where S_c = ultimate strength of the duplex alloy

S_m = ultimate strength of the martensite phase

S_f = stress in the ferrite at the ultimate tensile strain of the martensite

V_m = volume fraction of the martensite.

It is useful to rearrange the equation to facilitate correspondence to the graphical results as:

$$S_c = (S_m - S_f)V_m + S_f \ . \qquad (1a)$$

In this form, $(S_m - S_f)$ refers to the slope of the line, and S_f is the intercept at 0% martensite. The ultimate strength of the martensite is known to be strongly influenced by carbon content, and many researchers have derived equations relating strength to carbon content[15,20] by such methods as least squares analysis. It is generally accepted that S_m is proportional to $C^{1/3}$. The tensile strength of the ferrite is assumed to be constant for the following reasons:

a) the carbon content of the ferrite is essentially constant, and

b) the major strengthening mechanism of the ferrite, subgrain formation, is beleived to be constant also. Analysis of numerous transmission electron micrographs showed no significant differences in subgrain size from the intermediately quenched 1010 and 1020 steels, or at varying martensite percentages. Microhardness readings in the ferrite areas of numerous fractured tensile specimens were almost identical, and substantiate this result.

Equation 1 is derived for the conditions that the strong phase particles (martensite in this case) are unidirectionally aligned, and equally strained. These are clearly not the conditions in the duplex alloy, and any attempt to quantitatively relate to the equation would be empirical only.

The results of the tensile tests are shown in Figures 15 and 16, and assume an almost linear relation over the range of martensite fractions tested. The fact that this is not Equation 1 exactly can be shown easily. If $(S_m - S_f)$ is the slope of the line, it is constant. From previous discussions it is known that S_m varies significantly with carbon content while S_f is unchanged. Thus for the duplex system there is actually a small amount of curvature. The slope of the 1020 ultimate strength curve is slightly greater than for the 1010 curve, which reflects the higher strength of the 1020 martensite at equal volume fractions (carbon content is higher). Thus Equation 1 appears to be sensitive to the duplex system in this respect.

A serious omission from Equation 1 can be determined by examination of Figure 15 (1010 steel) with special attention to the ultimate strength curves. The large difference in the slopes $(S_m - S_f)$ can not be attributed to S_m because both steels are of the same overall composition, so at equal volume fractions, the carbon contents of the martensites are the same and the strengths are the same. From the previous discussion S_f is unchanged. Having eliminated or accounted for these aspects, attention is turned to the microstructural differences in the two. Examination by transmission electron micros-

copy has shown no morphological differences in the martensitic phases of the duplex structures obtained by continuous annealing or intermediate quenching. Some of the difference in slope may be assigned to the difference in the ferritic areas: the intermediately quenched material had a ferrite subgrain structure, whereas no observable division of the continuously annealed ferrite into subgrains occured. Extrapolation of the curves to 0% martensite shows a 42 ksi difference in S_f, which can not be totally attributable to the subgrain structure difference. The obvious dissimilarity is illustrated in the optical micrographs of Figure 3. C is from specimen CC (continuously annealed 1010) and D is from specimen 1B (intermediately quenched 1010). The shape of the martensitic regions [from the two processes] is drastically different, and becomes suspect as the cause for the different behaviors. Thus Equation 1 is inadequate and needs to be modified to include factors concerning the detailed morphology [size, shape and distribution] of the second phase in the duplex structure. This result differs from that found for duplex austenitic-martensitic steels.[34]

Tempering changes both S_m and S_f, and it is desirable to isolate, as much as possible, the effect of S_f. From Table 3 the change in S_m from the as quenched to the 200 °C tempered condition can be calculated for the fully martensitic specimens; at 0.1% C the change is 1% and at 0.19% C the change is 4%. Assuming a linear change, which is at least qualitatively reasonable it is possible to predict the tempering responses of higher carbon martensites (with 0.5% Mn) at 200 °C. A complicating factor that remains is that the

carbon content in the martensite cannot be determined accurately. Bain and Paxton[14] and Irvine[16] have related hardness values to carbon content of martensites containing up to 0.5% carbon, and the converted microhardness readings from the as quenched 1010 and 1020 martensites are in good agreement with the published figures. If a curve using the hardness values obtained for 1010 and 1020 is plotted parallel to that of Bain and Paxton, and the relationships of Figure 21A (upper drawing) are used, the carbon content in the martensites of the 1010 duplex structure can be estimated. The values obtained from such an estimation are tabulated below Figure 21. A rough, qualitative approximation of the effect of S_f on the strength of the duplex system becomes possible by making a comparison to a formula relating carbon to tensile strength, e.g., reference 15, and assuming a linear response to tempering at 200 °C.

Using the results obtained from the estimations and inserting the values (as relative magnitudes) in Equation 1 shows that for the tempered condition, the stress in the ferrite, S_f, decreases as the volume fraction of the ferrite decreases. Comparing the relative magnitudes of the contributing factors, i.e., $S_m V_m$ and $S_f(1 - V_m)$, ascertains the validity of the following: as V_m increases, the carbon content in the martensite decreases, therefore the ultimate strength of the martensite also decreases. However, the total martensite contribution to the duplex strength, S_c, increases. The stress in the ferrite decreases as the martensite fraction increases; the total contribution of the ferrite to the duplex strength also decreases.

It is emphasized that with so many approximations and assumptions that only a very limited estimate of the behavior is possible. Nevertheless, it can be seen that Equation 1 is a useful empirical equation to describe the mechanical properties of these duplex systems.

2. Qualitative Relationships.

It is immediately obvious from Figure 23 that the strength/ductility combinations of the intermediately quenched 1010 are superior to those of the continuously annealed alloy (1010 C). This can be attributed to the finer dispersion of martensite in the ferrite matrix, and to the ferrite subgrain strengthening. An advantage may also be assigned to the fewer fibrous carbides at the ferrite/martensite interfaces. With the relative inferiority of the continuously annealed 1010, the remainder of this correlation will concern only the intermediately quenched 1010 and 1020.

In both the 1010 and 1020 duplex steels, the network of subgrains was very obvious. Analysis of numerous transmission electron micrographs and general observations proved that the average subgrain spacing was approximately 0.5 microns for both steels, and appeared to be essentially independent of V_m. Thus, the strengthening variance due to subgrains is believed to be negligible.

There is much controversy in the literature concerning the beneficial aspects of retained austenite. Its ability to effectively inhibit crack growth has especially been contested. However, the amounts of retained austenite detected in the duplex alloys was very small, and the effect it would have on mechanical properties is

likewise expected to be very small. In any case, small amounts were detected in both 1010 and 1020, and at all volume fractions of martensite observed, and any property difference attributable to retained austenite is again expected to be negligible.

Similarly, the amount of autotempering was essentially independent of V_m and was observed in approximately equal amounts in 1010 and 1020. As mentioned previously, the prior austenitic grain size for all duplex alloys was ASTM #5. No significant strengthening differentials could thus be attributed to these metallurgical parameters.

While no deliberate effort was made to quantify the amounts of twinning in the duplex specimens, twinning seemed more prevalent in specimen 2B (1020) than in specimen 1B (1010). Kelly and Nutting[35] have shown that increased carbon and the subsequent lowering of M_s increased the probability of transformation twinning; an assertion corroborated by Thomas.[36] The martensite in 2B (V_m = 40%) is expected to be of considerably higher carbon content than that in 1B (V_m = 35%), and the limited experimental observations are thus supportive of the previous arguments. The effect of twinning on martensite toughness has been fairly well documented; for as quenched steels with the same carbon contents, fracture toughness decreases with increasing twinning.[37] Twinned martensites in carbon containing steels have also been shown to have inferior fracture toughness compared to untwinned martensites at the same strength level.[38] A comparison of the subsize charpy values vs. yield strength (Figure 22) shows the duplex 1020 to have

impact resistance which is considerably inferior to the duplex 1010. This is presumably due to the larger amounts of twinning in addition to the higher carbon content in the 1020.

The final variable to be considered appears to be the most influential. For a given steel, the volume fraction of martensite (and its carbon content) is seen to be the major controlling factor for the strength, ductility and impact resistance of the duplex material. Examination of Figures 15-17 and 19 supports this conclusion. With the other metallurgical variables equal, the higher carbon content in the 1020 martensite vs. the 1010 martensite at equal volume fractions is chiefly responsible for the differences in mechanical properties.

D. COMPARISON TO COMMERCIAL SPECIFICATIONS

Figure 23 shows the strength/ductility combinations obtained with the intermediately quenched, duplex 1010 and 1020 alloys in this investigation. Also shown are the tensile properties of the commercial 1010 and 1020 in the hot rolled and cold drawn conditions.

Extrapolation of the curves shows that the properties obtained with the duplex steels meet or exceed the commercial specifications (compose the as quenched to the cold drawn, and the tempered to the hot rolled), without the need for thermomechanical treatment. The strengths obtained in this investigation greatly exceed the strengths of commercial 1010 and 1020, with the consequent sacrifice in ductility. As mentioned previously, the final selection of properties is determined

by the application for which the steel will be used.

There are no commercial specifications available for 1010 and 1020 impact values, and typical values could not be found in the literature for comparison.

IV. CONCLUSIONS

Based on the investigations and characterizations of the fully martensitic and duplex 1010 and 1020 steels in this research, the following conclusions are made:

1. The rule for two phase mixtures, $S_c = S_m V_m + S_f(1 - V_m)$, may be used empirically to describe the mechanical properties of these duplex alloys. Suitable modifications to include the size, shape and distribution of the second phase are necessary for more quantitative correlations.
2. For the 1010 steel, the intermediate quench route enables strength/ductility combinations to be obtained that are superior to those obtained by continuous annealing.
3. The largest factor controlling the strength, ductility and impact resistance of the duplex alloys in this investigation is the volume fraction of martensite.
4. The property differentials between the duplex 1010 and 1020 (intermediately quenched) at equal volume fractions of martensite are due mainly to the higher carbon content (hence, higher strength) of the 1020 martensite.
5. Using the average energy criterion, the ductile-brittle transition temperature for the fully martensitic and duplex 1020 steels is about 25 °C. The DBTT appeared to be essentially independent of V_m.

6. It is suggested that the poorer impact properties of the duplex 1020 steel (compared to 1010) are attributable to the large amounts of transformation twinning and higher carbon content in the 1020.
7. The tensile properties of the duplex 1010 and 1020 steels in this investigation meet or exceed commercial specifications, without the need for thermomechanical treatment.

REFERENCES

1. Technology Forecast, Metal Progress, p. 32, Jan. (1977).
2. J. Y. Koo and G. Thomas, Mat. Sci. and Eng., 24, 187 (1976).
3. J. Y. Koo and G. Thomas, Met. Trans., 8A, 525 (1977).
4. J. Y. Koo, M.S. Thesis, University of California, Berkeley, LBL-3587, Feb. (1975).
5. S. Hayami and T. Furukawa, Micro Alloying '75, Symposium on High Strength, Low Alloy Steels, Products and Processes, p. 78, Washington, D.C. (1975).
6. R. L. Cairns and J. A. Charles, J. Iron and Steel Inst., p. 1044 (1967).
7. M. Enomoto and E. Furubayashi, Mat. Sci. and Eng., 24, 123 (1976).
8. S. K. Hwang, M.S. Thesis, University of California, Berkeley, LBL-3503, Dec. (1974).
9. S. Jin, S. K. Hwang and J. W. Morris, Jr., Met. Trans., 6A, 1721 (1975).
10. R. L. Miller, Met. Trans., 3, 905 (1972).
11. E. Snape and N. L. Church, J. of Metals, p. 23, Jan. (1972).
12. R. A. Grange, Met. Trans., 2, 65 (1971).
13. Automotive Engineering, 84, 49, Nov. (1976).
14. Edgar C. Bain and Harold W. Paxton, Alloying Elements in Steel, American Society For Metals, Metals Park (1966).
15. W. H. McFarland, Trans. TMS-AIME, 233, 2028 (1965).
16. K. J. Irvine, J. Iron and Steel Inst., p. 820 (1962).

17. Annual Book of ASTM Standard, designation E23-72, sections 8.2.1 and 8.2.2, revised June (1972).

18. Robert DeHoff and Frederick Rhines, Quantitative Microscopy, McGraw-Hill, New York (1968).

19. M. Hansen, Constitution of Binary Alloys, 2nd Ed., McGraw-Hill, New York (1958).

20. G. R. Speich and H. Warlimont, J. Iron and Steel Inst., p. 385 (1968).

21. A. S. Tetelman and A. J. McEvily, Jr., Fracture of Structural Materials, John Wiley and Sons, New York (1967).

22. G. R. Speich and W. C. Leslie, Met. Trans., 3, 1043 (1972).

23. Paul G. Shewmon, Transformations in Metals, McGraw-Hill, New York (1969).

24. H. I. Aaronson, H. A. Domian and G. M. Pound: Trans. AIME, 236, 753 (1966).

25. H. W. Paxton, "Transformation and Hardenability in Steels", Climax Molybdenum Co., Ann Arbor, Mich., p. 3, 1967.

26. D. H. Warrington, J. Iron and Steel Inst., p. 610, July (1963).

27. K. Campbell and R. W. K. Honeycombe, Metal Science, 8, 197 (1974).

28. G. Krauss and A. R. Marder, Met. Trans., 2, 2343 (1971).

29. S. K. Das and G. Thomas, Met. Trans., 1, 325 (1970).

30. C. A. Apple, R. N. Caron and G. Krauss, Met. Trans., 5, 593 (1974).

31. B. V. N. Rao, J. Y. Koo and G. Thomas, Proc. 33rd Electron Microscopy Soc. Am., Claitors, Baton Rouge (1975), p. 30.

32. J. Y. Koo, Ph.D. Thesis, in progress.

33. N. J. Petch, Progr. in Metal Phys., 5, 1 (1954).

34. P. R. Manganon and G. Thomas, Met. Trans. 1, 1587-1594 (1970).

35. P. M. Kelly and J. Nutting, Proc. Royal Soc., A259, 45 (1960).

36. G. Thomas, Met. Trans., 2, 2373 (1971).

37. J. McMahon and G. Thomas, 3rd Int. Conf. on Strength of Metals and Alloys, Cambridge, England, 1, 180 (1973).

38. S. K. Das and G. Thomas, Trans. ASM, 62, 659 (1969).

Table I. Alloy compositions determined after austenitization (wt. %)

Alloy 1	(1010)	Carbon	0.10	Manganese	0.5
Alloy 2	(1020)	Carbon	0.19	Manganese	0.5

Table II. Mechanical Properties (as quenched)

	Treatment	Designation	Two Phase Temperature (°C)	V_m	Yield Strength ksi	Yield Strength (MPa)	Ultimate Strength ksi	Ultimate Strength (MPa)	e_u (%)	e_u (%)	Room Temperature Charpy Energy fullsize	Room Temperature Charpy Energy (Ft-Lbs) subsize
1010	A+TP	1A	775	30	64	(442)	99	(683)	10	15		11
	A+TP	1B	795	35	66	(455)	104	(718)	9.5	14		11
	A+TP	1C	815	45	79	(545)	113	(780)	8.5	13		8
	A	1M	-	100	124	(856)	144	(994)	4	8		15
	A+CTP	CA	765	30	68	(470)	110	(760)	8	11		
	A+CTP	CB	775	40	69	(477)	108	(746)	7	10		
	A+CTP	CC	795	55	76	(525)	111	(767)	5	8		
	A+CTP	CD	810	60	80	(552)	116	(801)	4	7		
	A+CTP	CE	740	15	68	(470)	105	(725)	10	13		
1020	A+TP	2A	725	25	57	(393)	96	(662)	10	14	21	2.5
	A+TP	2B	740	40	73	(504)	122	(842)	8.5	12	8.5	1.5
	A+TP	2C	755	50	75	(518)	127	(876)	7.5	11.5	6	1
	A	2M	-	100	170	(1173)	203	(1401)	4	8	26	8.5

A - Austenization at 1100 °C, agitated iced brine quench.
A+TP - Austenization followed by two phase annealing with intermediate quenching.
A+CTP - Austenization followed by continuous two phase annealing.

Table III. Mechanical properties (tempered 30 min. at 200 °C)

Designation		Yield Strength ksi	Yield Strength (MPa)	Ultimate Strength ksi	Ultimate Strength (MPa)	e_u (%)	e_t (%)
1010	1A2	51	(352)	80	(552)	12	21
	1B2	53	(366)	83	(573)	10	17
	1C2	54	(373)	84	(580)	8.5	16
	1M2	126	(869)	143	(987)	5.5	9
1020	2A2	50	(345)	77	(531)	13	19
	2B2	58	(400)	95	(656)	11.5	15
	2C2	65	(449)	104	(718)	10	13
	2M2	164	(1132)	195	(1346)	5	9

Table IV. Mechanical properties after tempering at 200, 400 and 600 °C

	Tempering Temperature (°C)	Yield Strength ksi	Yield Strength (MPa)	Ultimate Strength ksi	Ultimate Strength (MPa)	e_u (%)	e_t (%)
1010 (V_m=35)	As Quenched	66	(455)	104	(718)	9.5	14
	200	53	(366)	83	(573)	10	17
	400	52	(359)	74	(510)	11	18
	600	47	(324)	63	(434)	12	19
1020 (V_m=40)	As Quenched	73	(504)	122	(842)	8.5	12
	200	58	(400)	95	(656)	11.5	15
	400	56	(386)	82	(566)	16	25
	600	55	(379)	71	(490)	18	27

Table V. Impact testing of fullsize 1020 for transition temperature

		Temperature (C)					
		-75	-50	-25	0	23	90
specimen	2A		4	11	18	21	35
	2B		4	5	5.5	8	18
	2C		3.5	4	4	6	16
	2M	11	11	14	20	26	36

FIGURE CAPTIONS

1. Schematics of heat treatments. (a) and (b) intermediate quenching. (c) continuous annealing (1010 only).
2. Specimen geometries for mechanical testing specimens.
3. Optical micrographs. A, starting microstructure (1010 and 1020 were identical). B, 1020 duplex-intermediate quenching. C, 1010 duplex, continuous annealing. D, 1010 duplex, intermediate quenching.
4. Composite transmission electron micrograph of martensite lath embedded in the ferrite of specimen 2B (1020). Note the subgrain structure in ferrite.
5. Transmission micrographs of specimen 2B. A, martensite and dislocated ferrite. B, subgrain network. C, dislocations rearranged to form a subboundary. Some background precipitation (not identical) appears in some areas.
6. Transmission micrographs. Fibrous carbides at ferrite/martensite interfaces. A, bright field of specimen cc (continuously annealed 1010), B is the corresponding dark field. C, specimen 1C, intermediately quenched 1010.
7. Scanning electron fractographs of tensile failures of intermediately quenched specimens. All specimens showed a predominantly ductile failure. A and B, as quenched. C, tempered at 200 °C for 30 minutes.

8. Scanning electron fractographs at increasing magnifications continuously annealed 1010. Localized dual modes of failure are evident as shown in C and D.

9. Transmission electron micrographs. A, composite showing broad face of martensite lath. Note pocket boundaries and auto-tempering. B, typical lath martensite in 1010 and 1020 steels. C, complex intersection of laths in martensitic phase of duplex specimen.

10. Transmission micrographs. Extensive autotempering in completely martensitic structures of 1010 and 1020 steels.

11. Transmission micrographs of retained austenite in specimen 2M (1020). A, bright field. B, corresponding dark field where thin films of retained austenite reversed contrast when $(002)_\gamma$ reflection was imaged. C, selected area diffraction pattern. D, indexed SAD proving K-S relationship of martensite and austenite.

12. Transmission micrographs of specimen 2B (1020). A, dislocated ferrite and ferrite/martensite interface. Note twins at upper right. B, extremely fine transformation twins.

13. SEM fractographs of charpy failures at room temperature. Most failures may be characterized by quasi cleavage. Note: only intermediately quenched specimens were tested in impact.

14. SEM fractographs of charpy failures. A and B, room temperature fractures. C, secondary cracking in 2B at -50 °C.

15. Strength and elongation ductility vs. martensite fraction of intermediately quenched and continuously annealed 1010. Open and closed figures delineate yield and tensile strengths, unform and total elongations. Note: No continuously annealed material was tempered.

16. Strengths and elongation ductility vs. martensite fraction for intermediately quenched 1010 and 1020 steels. As quenched.

17. Strength and elongation ductility vs. martensite fraction for intermediately quenched 1010 and 1020 steels tempered at 200 °C for 30 minutes.

18. As quenched and tempered properties of intermediately quenched 1010 and 1020 steels containing 35% and 40% martensite, respectively.

19. Charpy impact energies of intermediately quenched 1010 (subsize) and 1020 (subsize and fullsize) steels.

20. Ductile-brittle transition curves for fully martensitic and duplex 1020 steels.

21. Plot of microhardness readings (vs. % martensite) in the martensitic phase of continuously annealed duplex specimens. Approximate carbon contents vs. martensite fraction are tabulated below the figure.

22. Charpy impact energies vs. yield strength for intermediately quenched 1010 and 1020 steels.

23. Total elongations vs. ultimate strengths of the 1010 and 1020 steels in this investigations. Also shown are the minimum commercial specifications of hot rolled and cold drawn 1010 and 1020 steels.

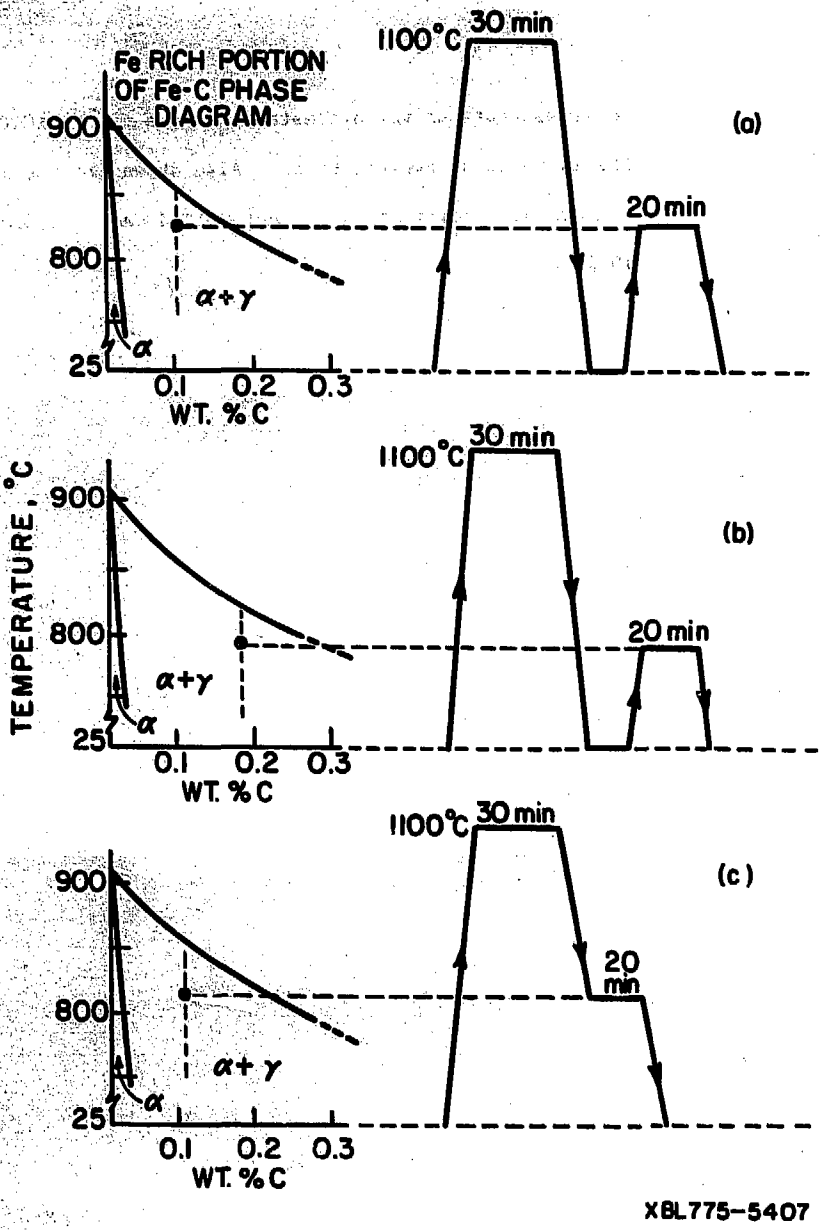
Fe RICH PORTION
OF Fe-C PHASE
DIAGRAM
1100°C
30 min
20 min
(a)
(b)
(c)
20
min
900
800
25
α+γ
α
0.1
0.2
0.3
WT. % C
TEMPERATURE, °C
XBL775-5407

Fig. 1

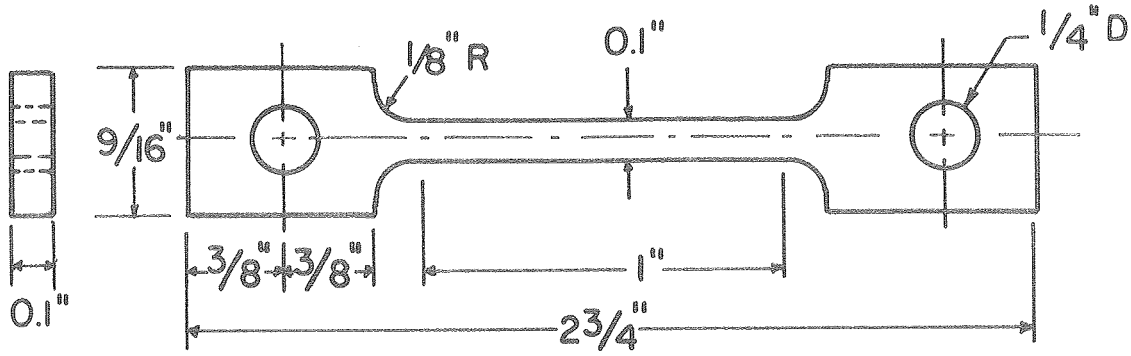

A. FLAT TENSILE SPECIMEN

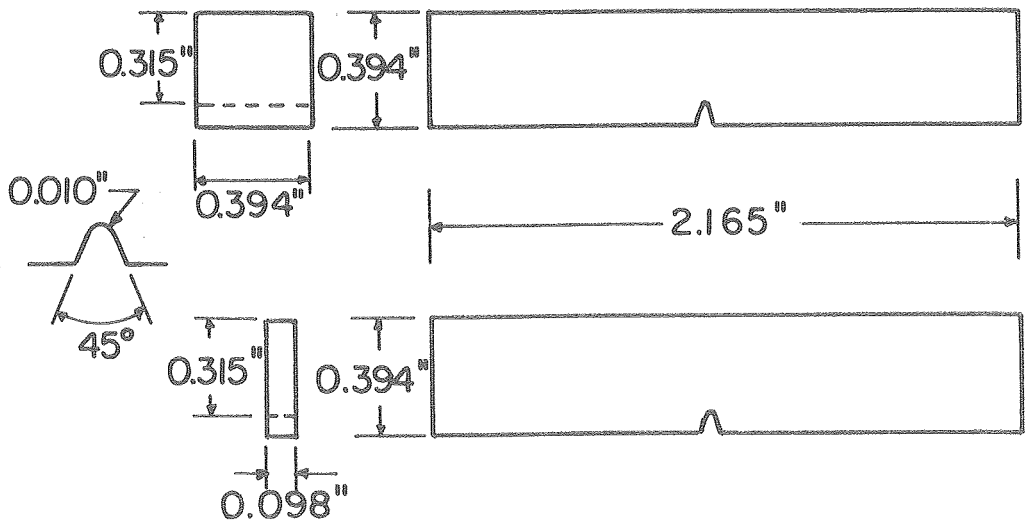

B. STANDARD AND SUBSIZE CHARPY V-NOTCH IMPACT SPECIMENS

XBL 775-5406

Fig. 2

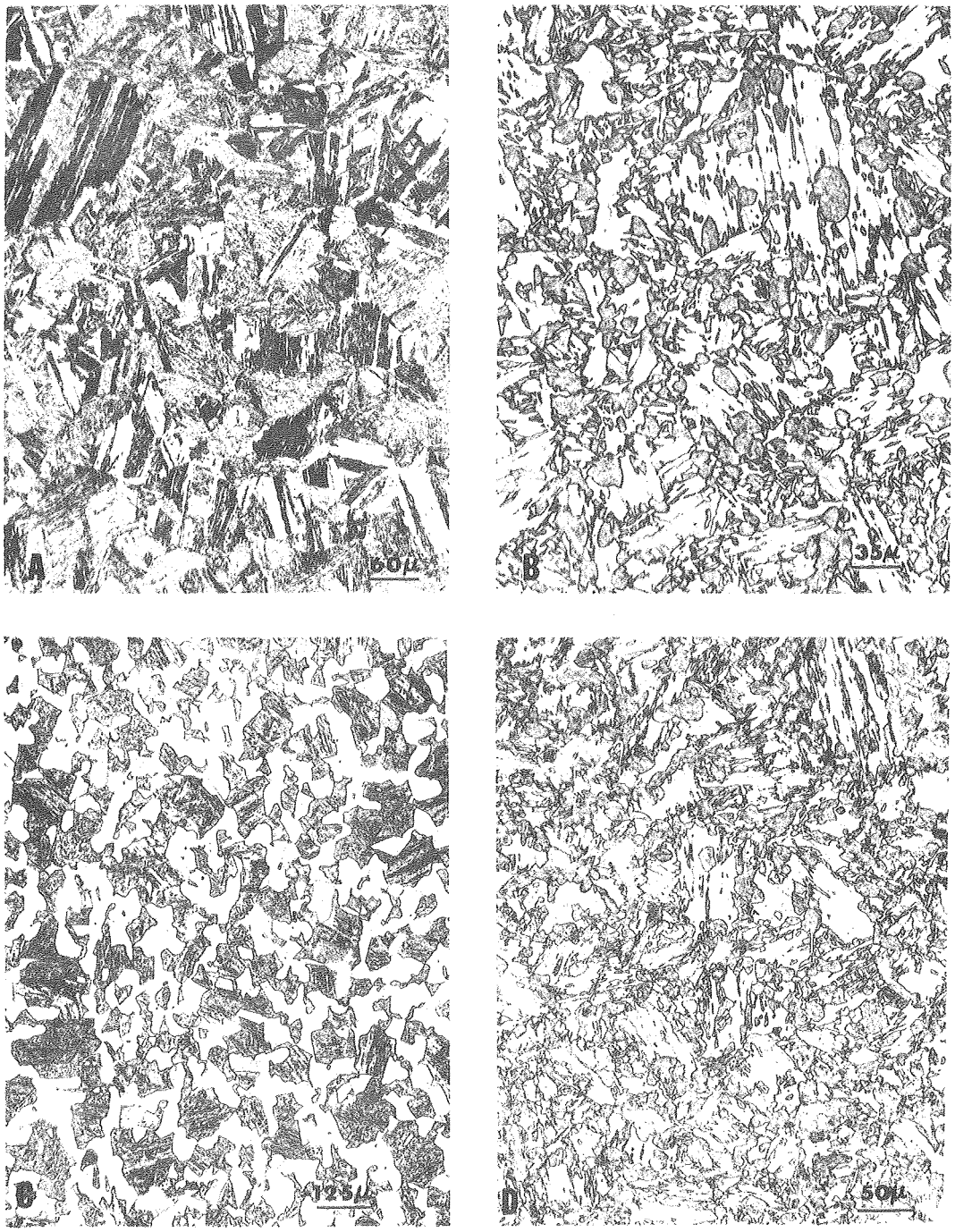

XBB774-4016

Fig. 3

0 0 0 0 4 8 0 4 9 1 8

XBB774-4009

Fig. 4

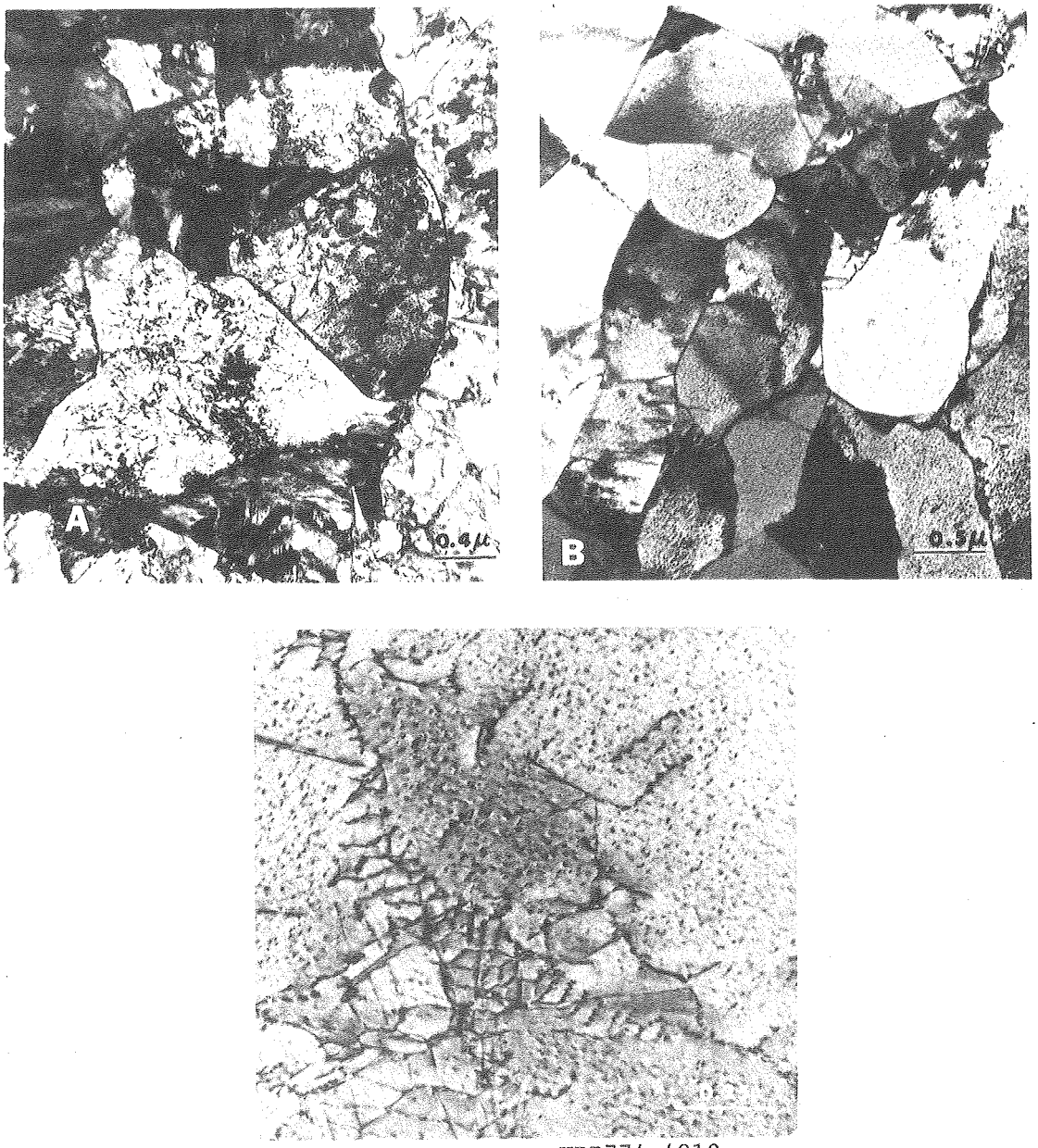

XBB774-4012

Fig. 5

0 0 0 0 4 8 0 4 9 1 9

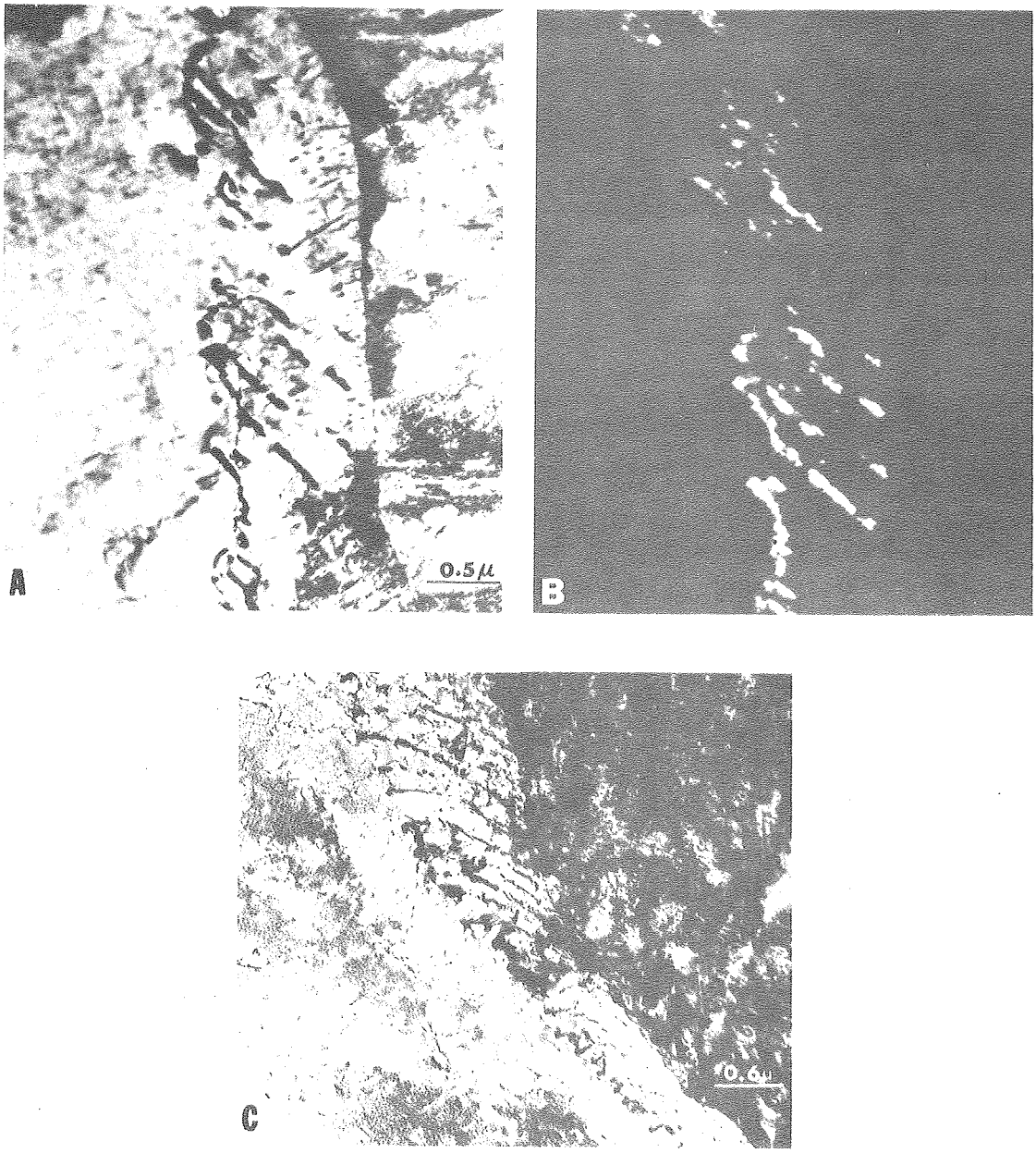

XBB774-4014

Fig. 6

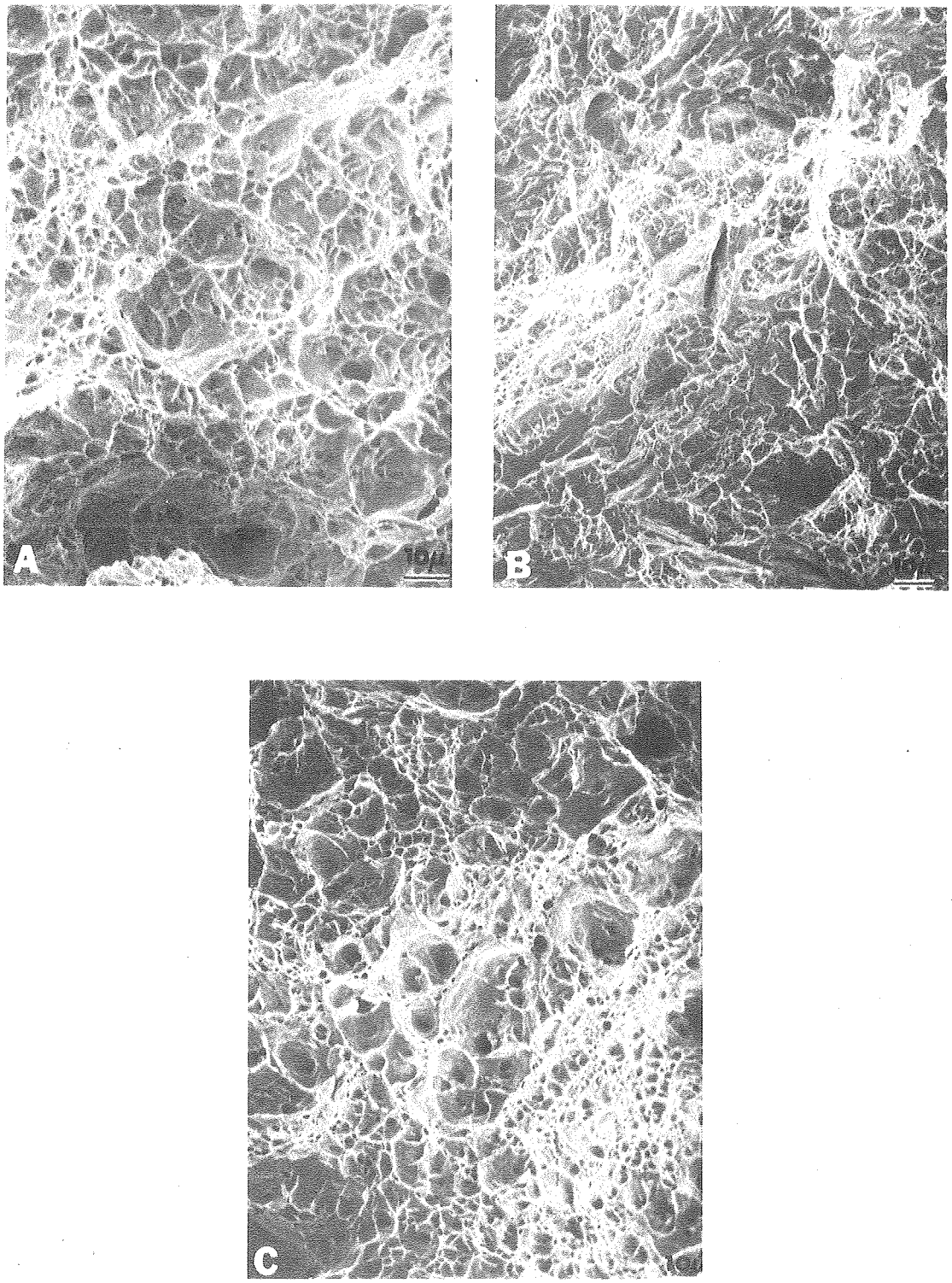

XBB774-4018

Fig. 7

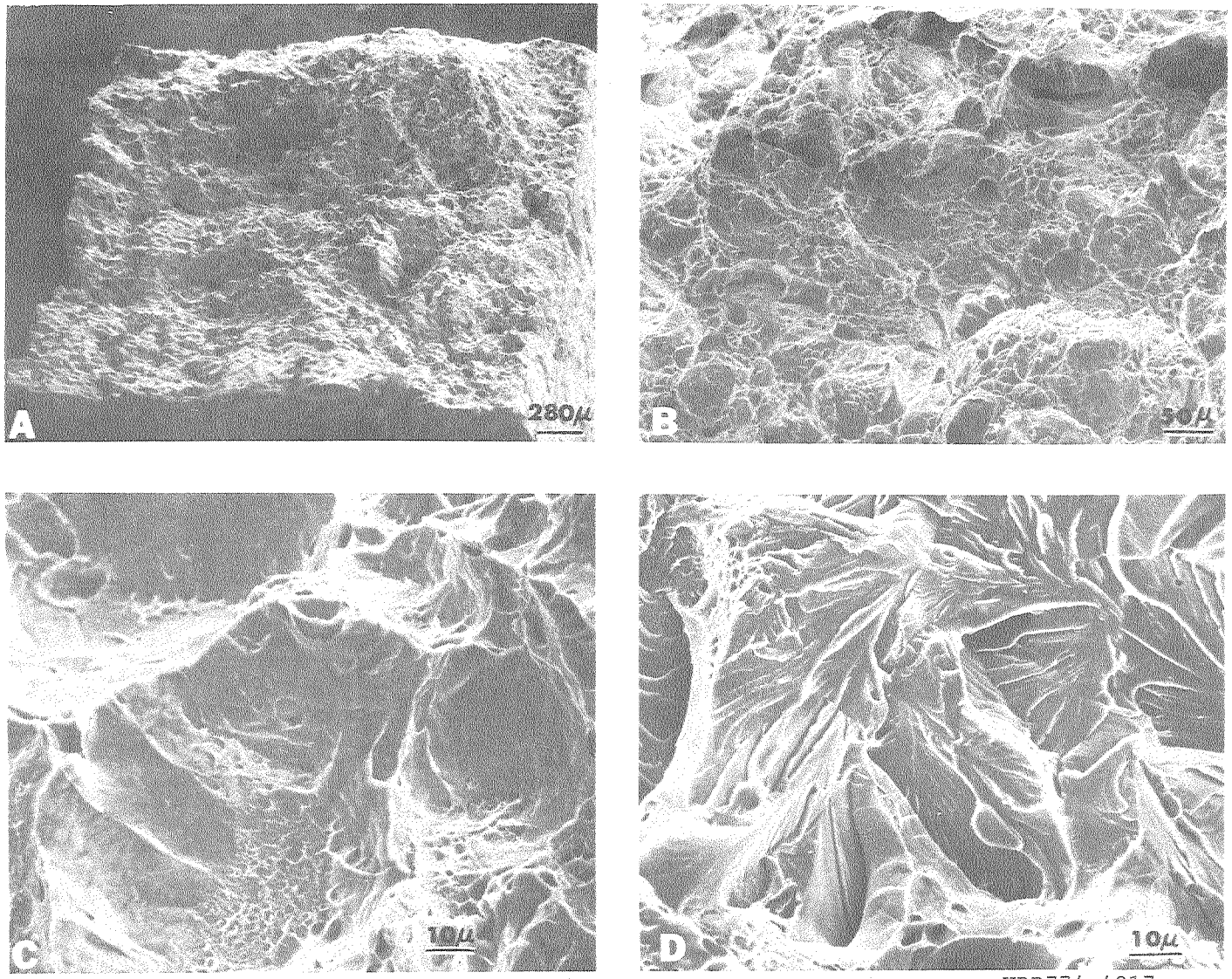

XBB774-4017

Fig. 8

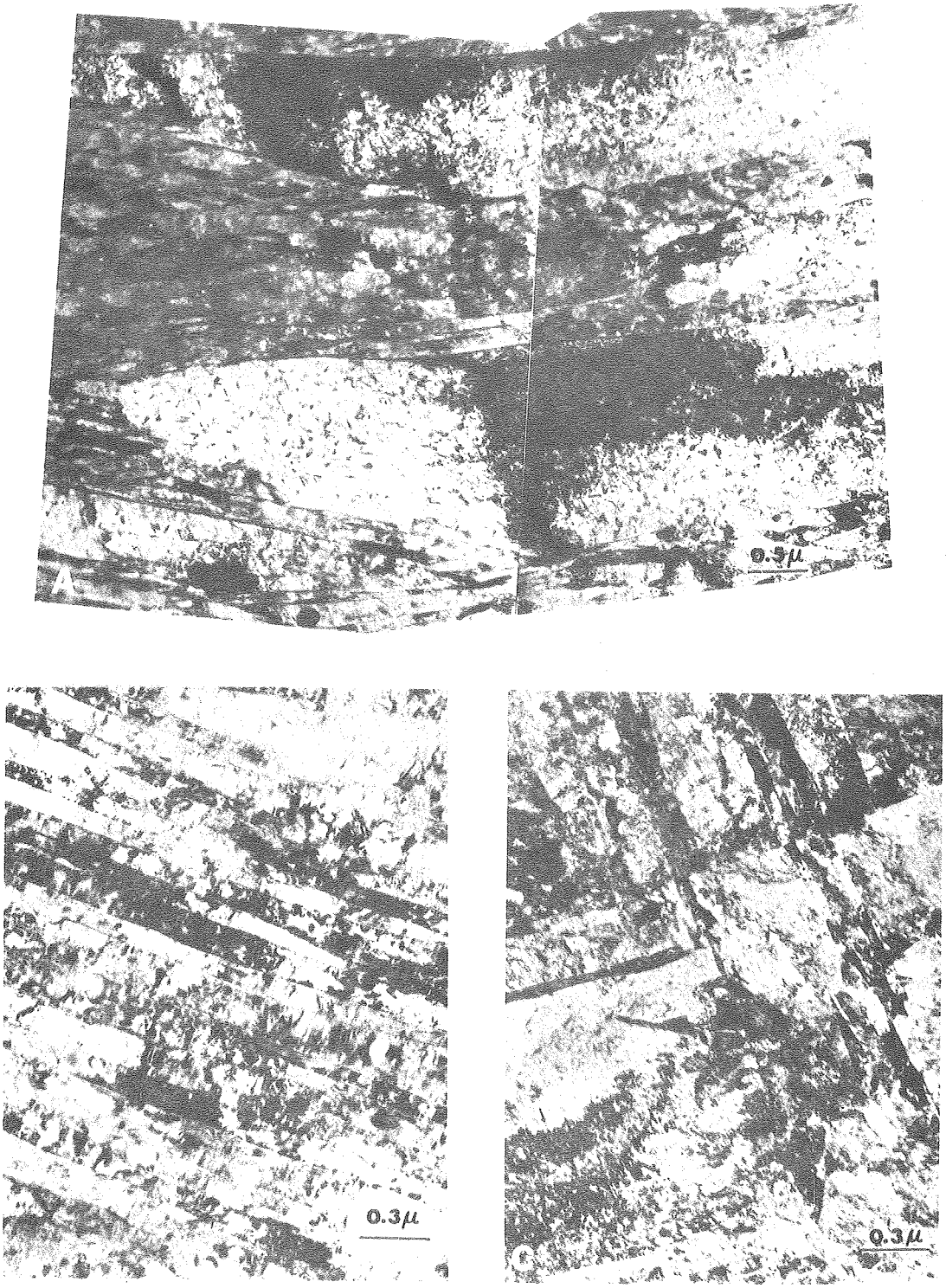

XBB774-4010

Fig. 9

0 0 1 0 4 8 0 4 9 2 0

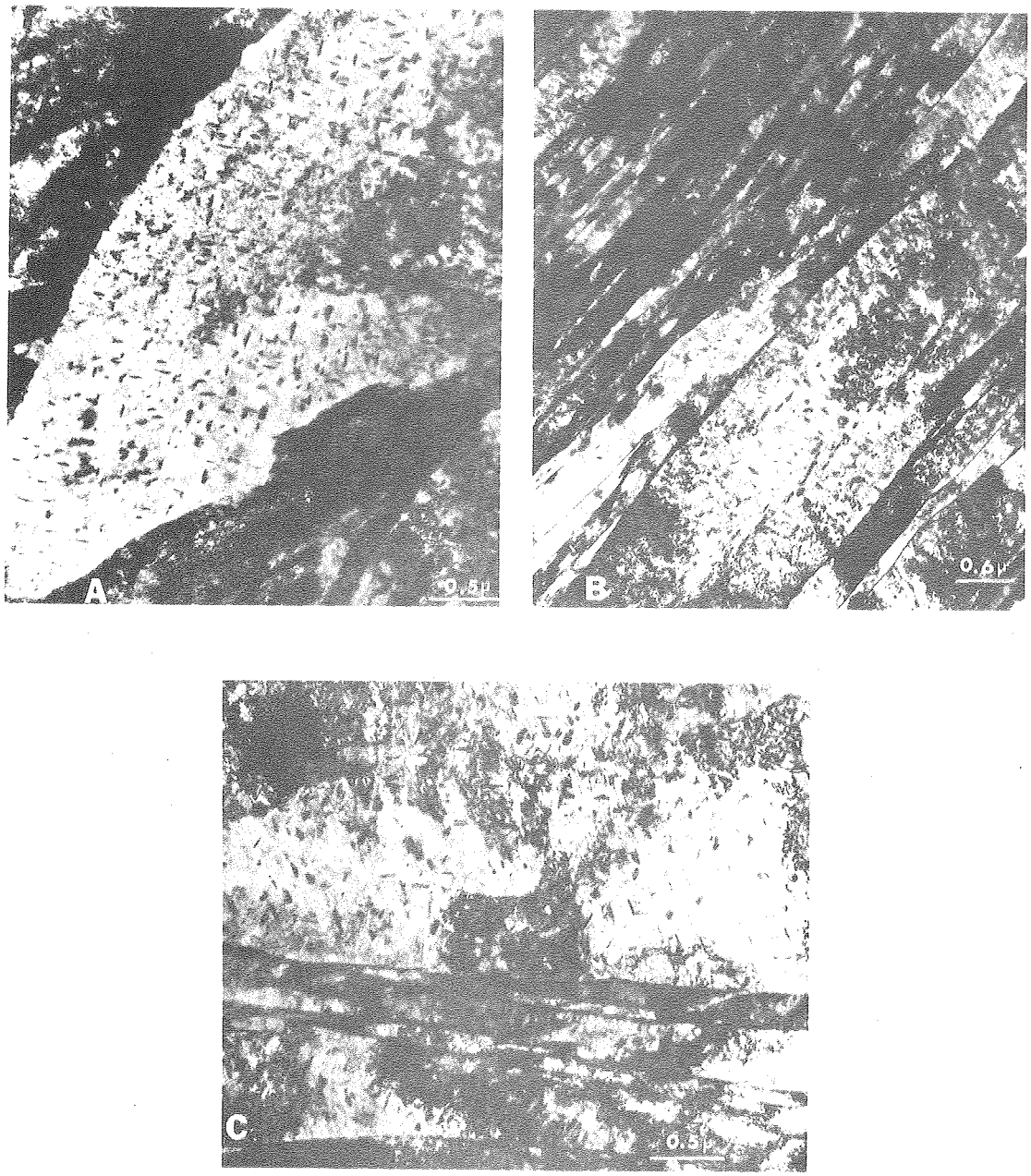

XBB774-4013

Fig. 10

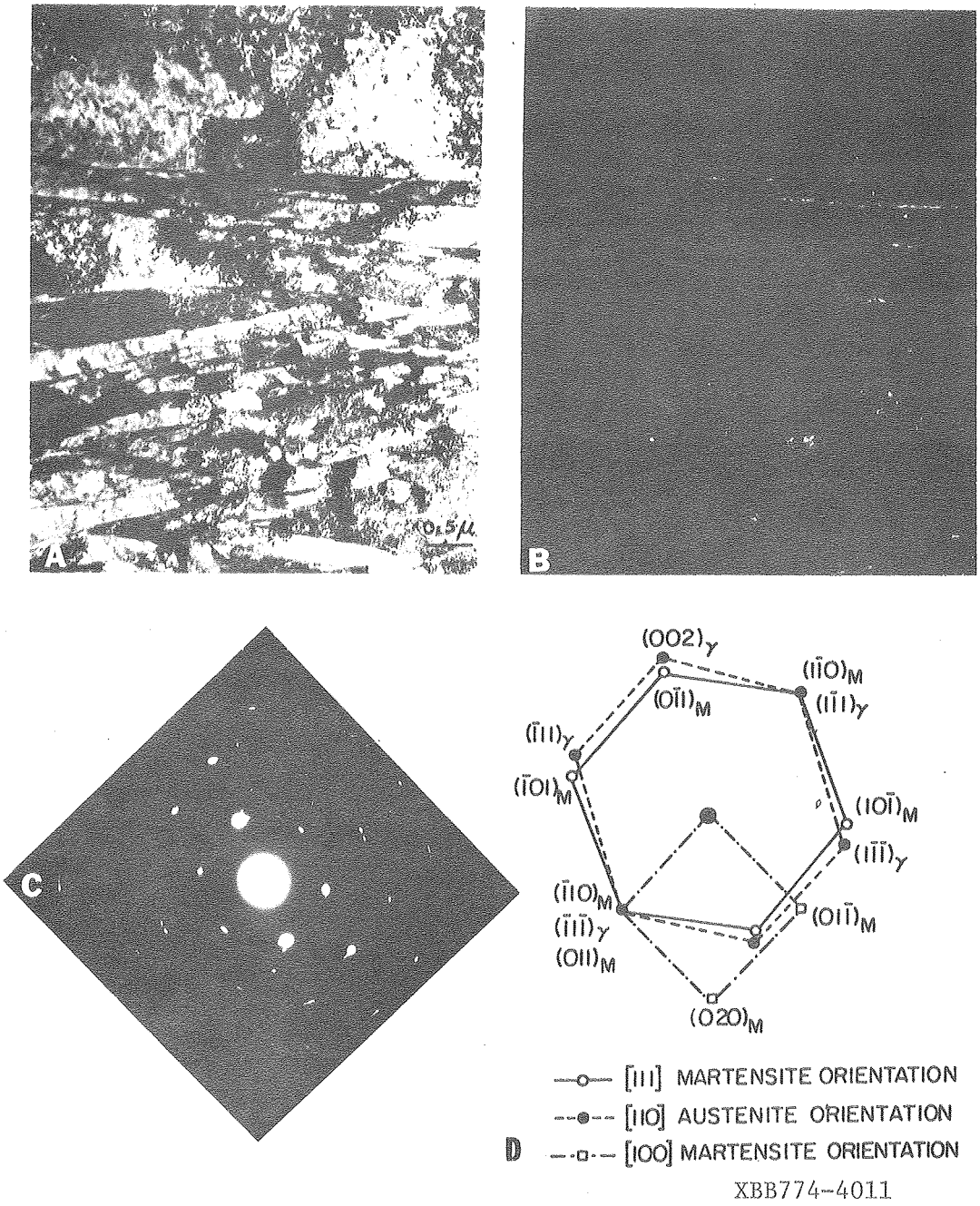

XBB774-4011

Fig. 11

0 0 0 0 4 8 0 4 9 2 1

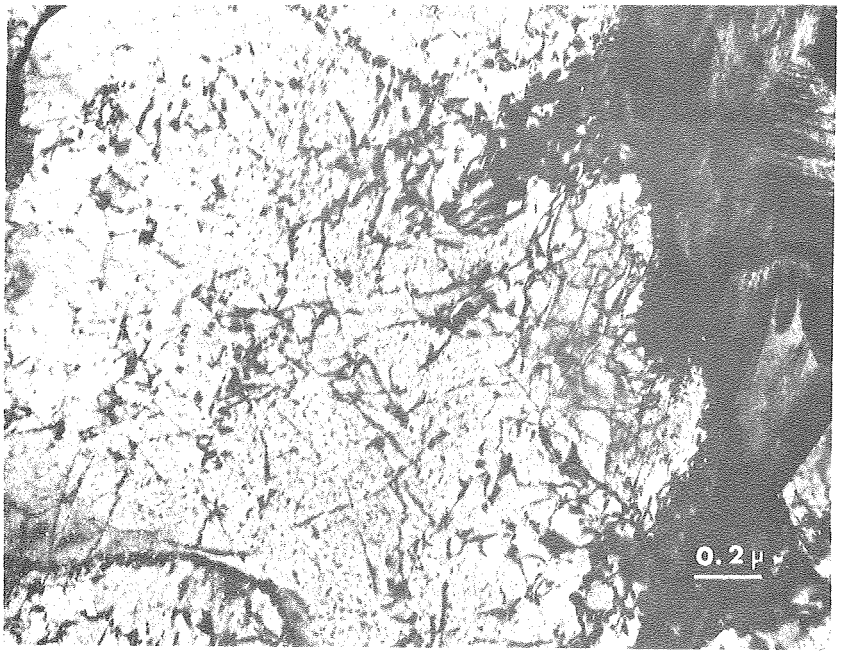

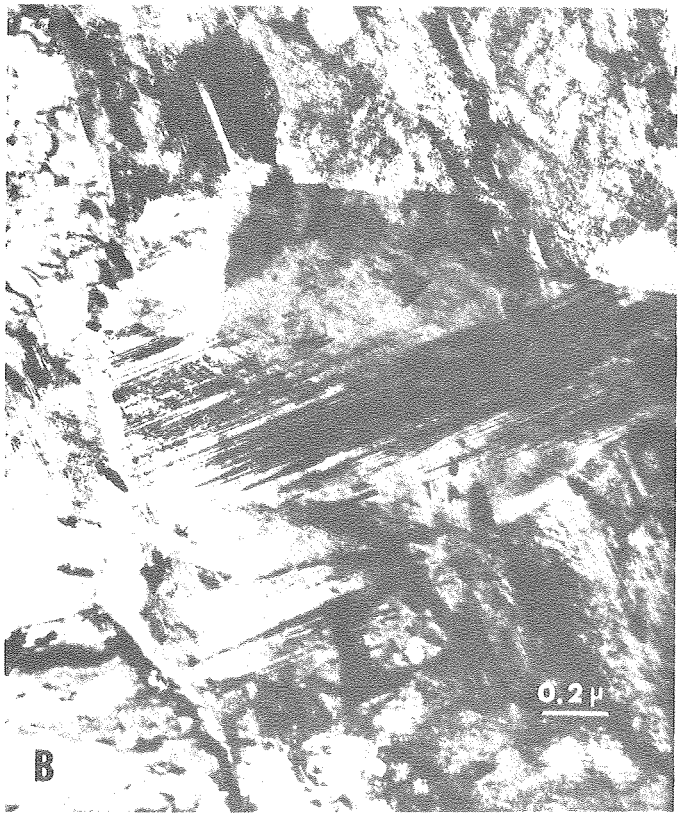

XBB774-4015

Fig. 12

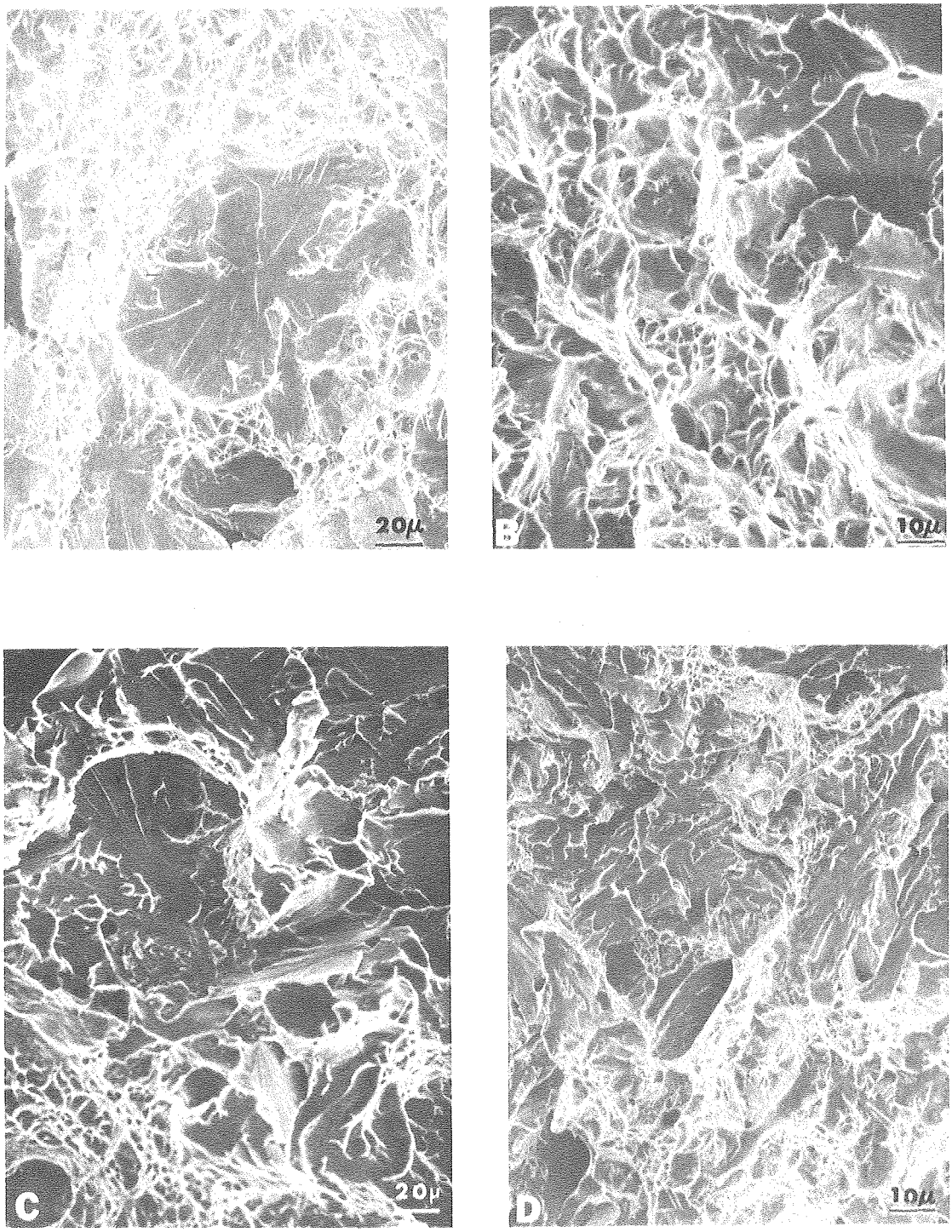

XBB774-4033

Fig. 13

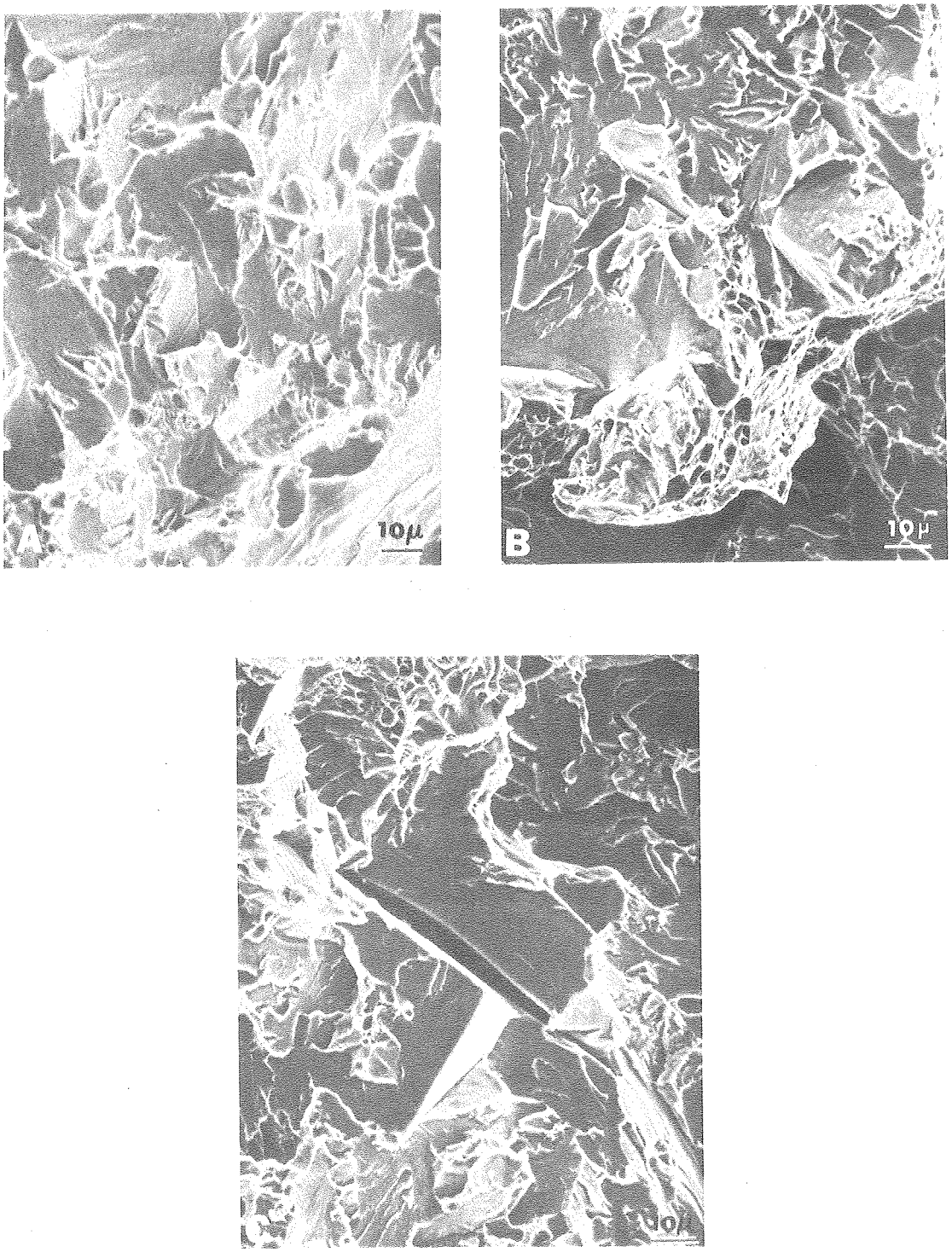

XBB774-4019

Fig. 14

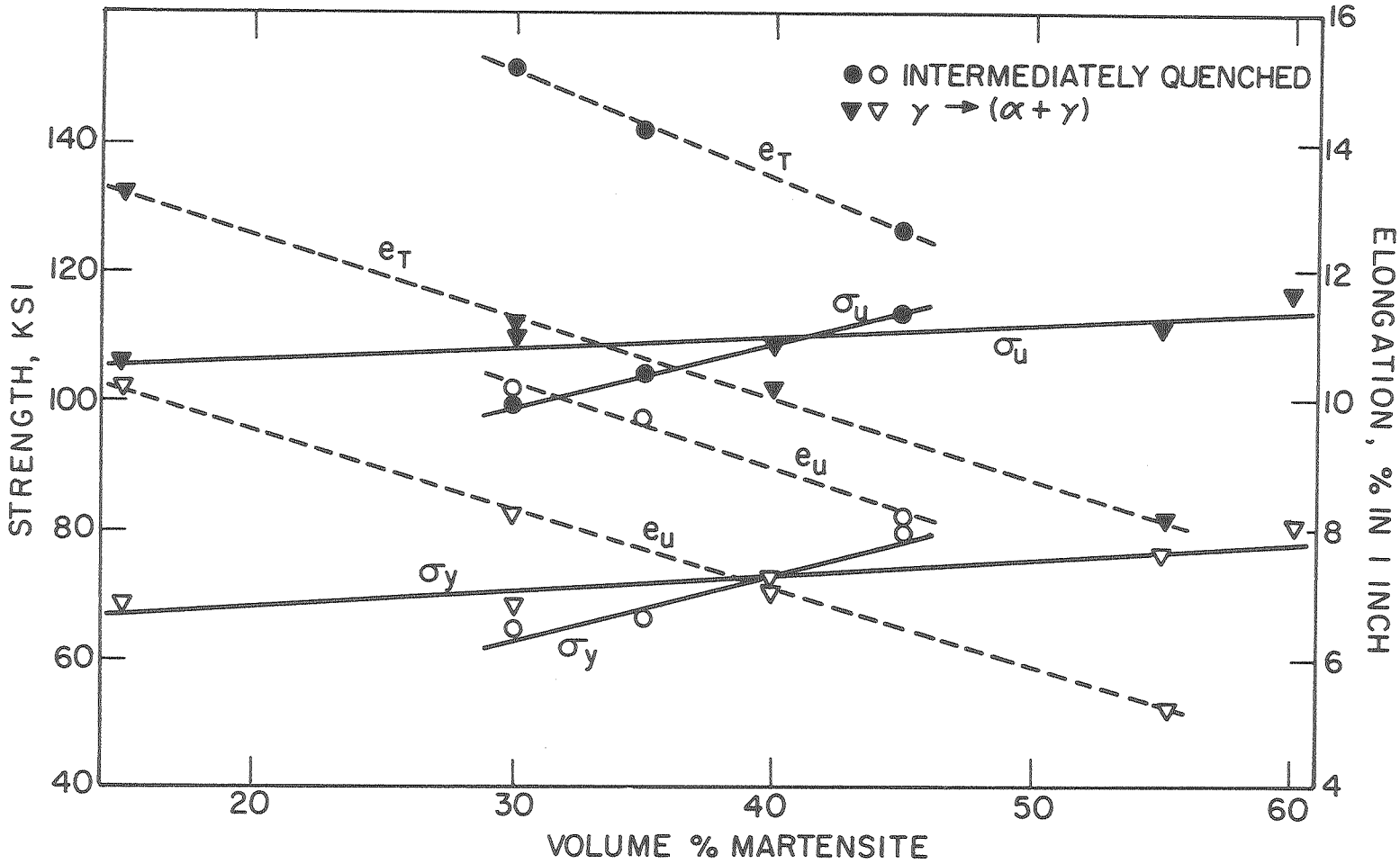

XBL 775-5411

Fig. 15

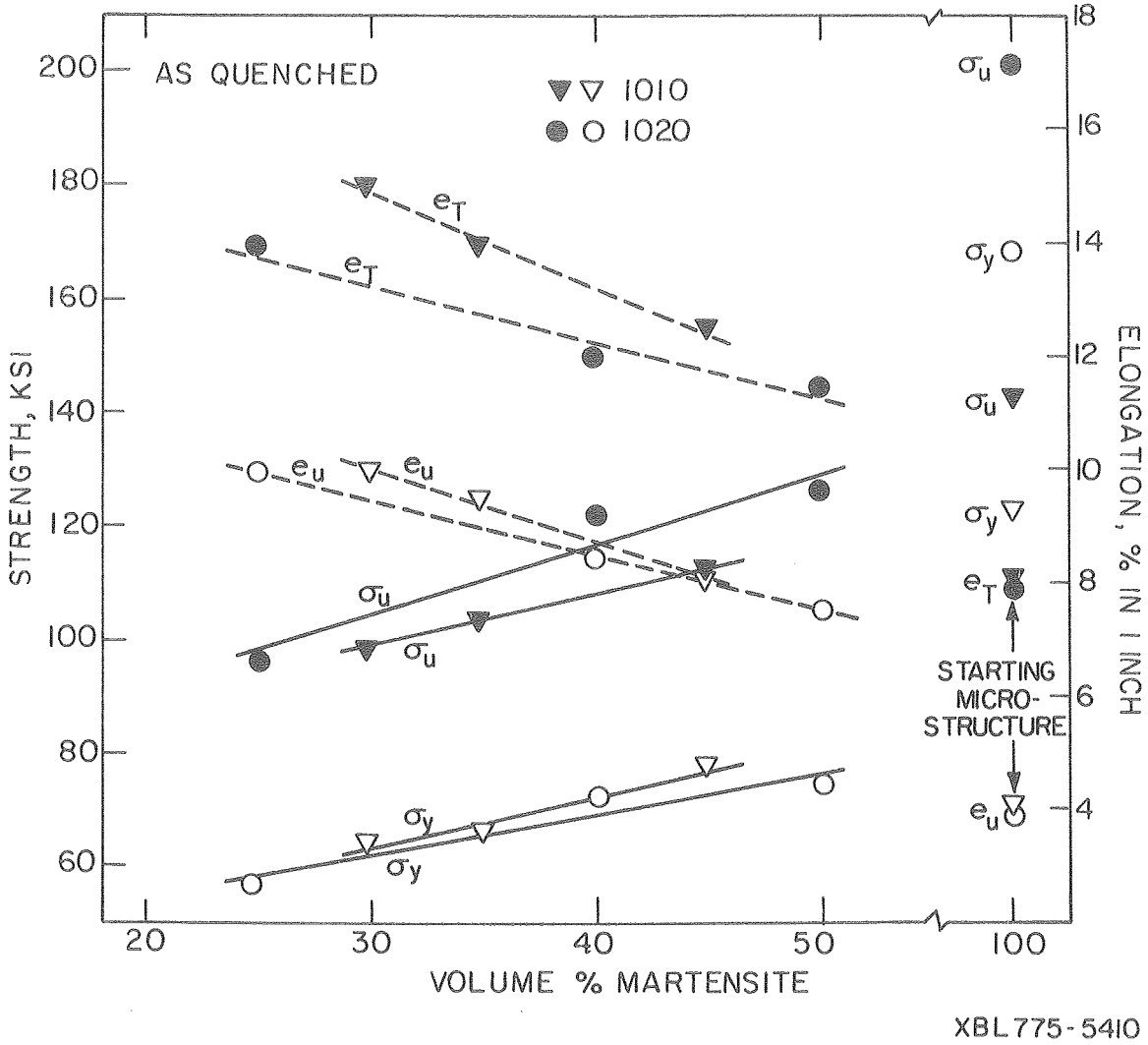
AS QUENCHED
1010
1020
STRENGTH, KSI
ELONGATION, % IN 1 INCH
VOLUME % MARTENSITE
STARTING MICRO-STRUCTURE
XBL775-5410

Fig. 16

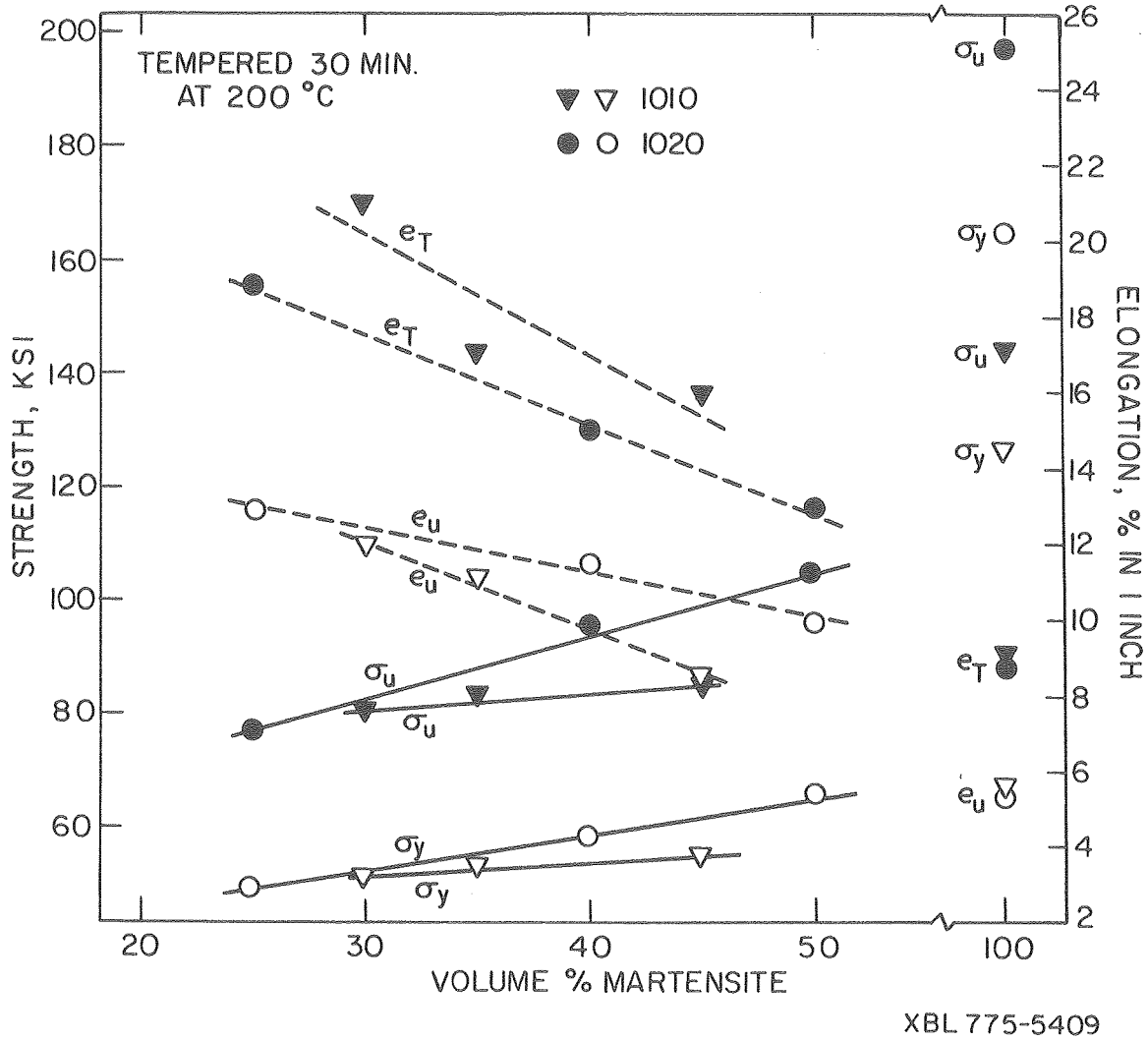
TEMPERED 30 MIN.
AT 200 °C
1010
1020
STRENGTH, KSI
ELONGATION, % IN 1 INCH
VOLUME % MARTENSITE
200
180
160
140
120
100
80
60
26
24
22
20
18
16
14
12
10
8
6
4
2
20
30
40
50
100
e_T
e_u
σ_u
σ_y
XBL 775-5409

Fig. 17

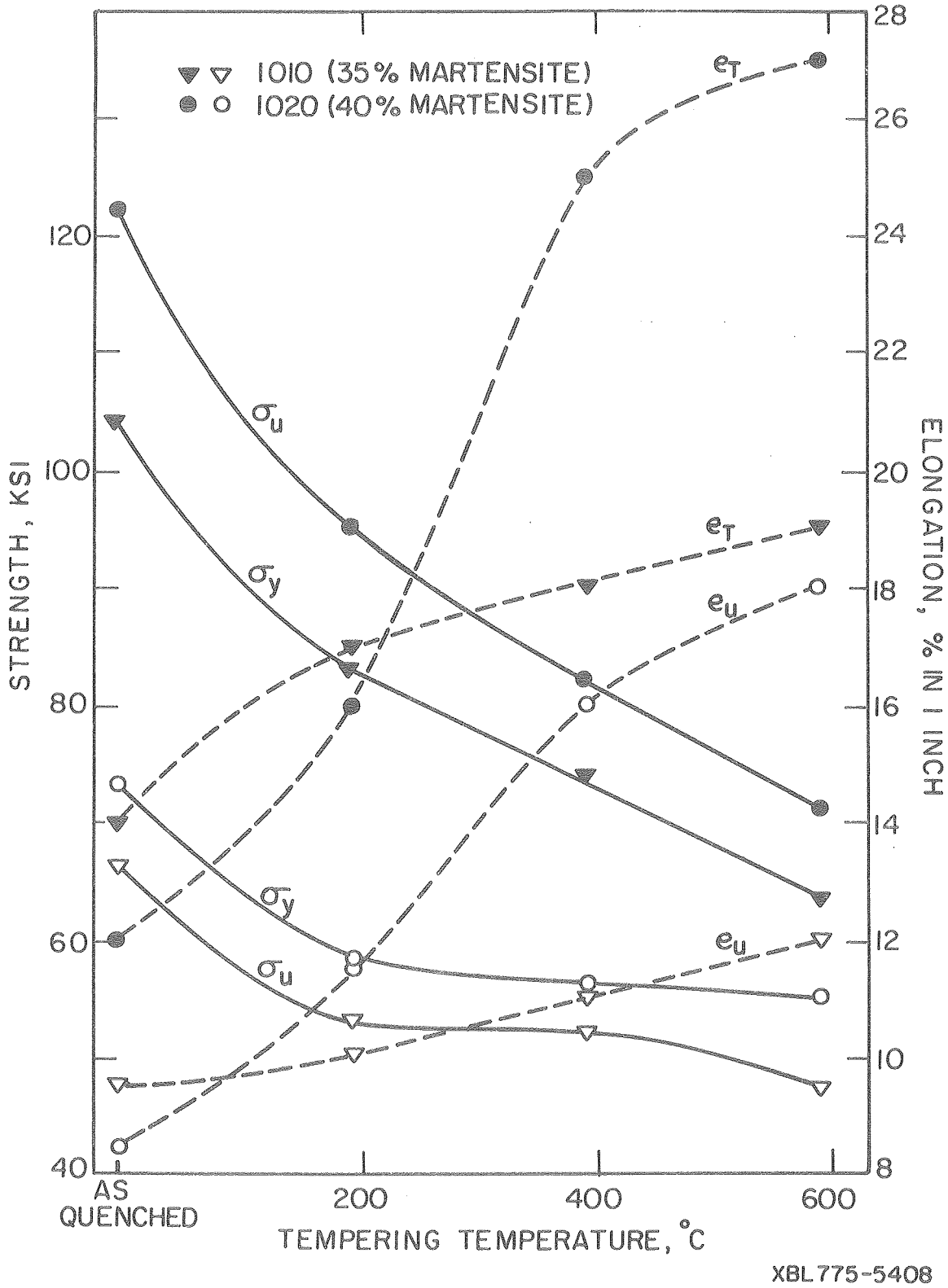
1010 (35% MARTENSITE)
1020 (40% MARTENSITE)
e_T
σ_u
σ_y
e_u
STRENGTH, KSI
ELONGATION, % IN 1 INCH
TEMPERING TEMPERATURE, °C
AS QUENCHED
200
400
600
40
60
80
100
120
8
10
12
14
16
18
20
22
24
26
28
XBL 775-5408

Fig. 18

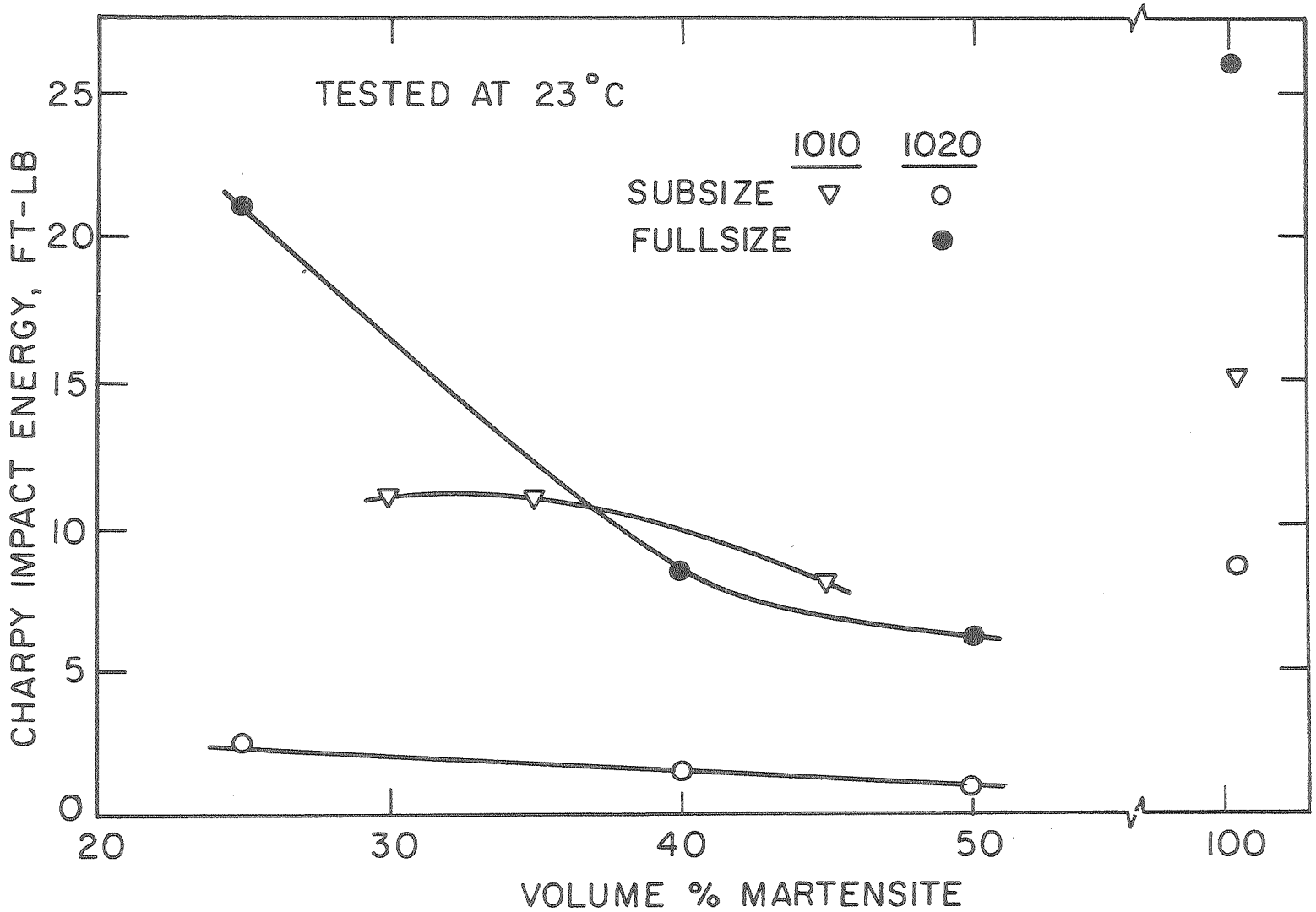

XBL775-5414

Fig. 19

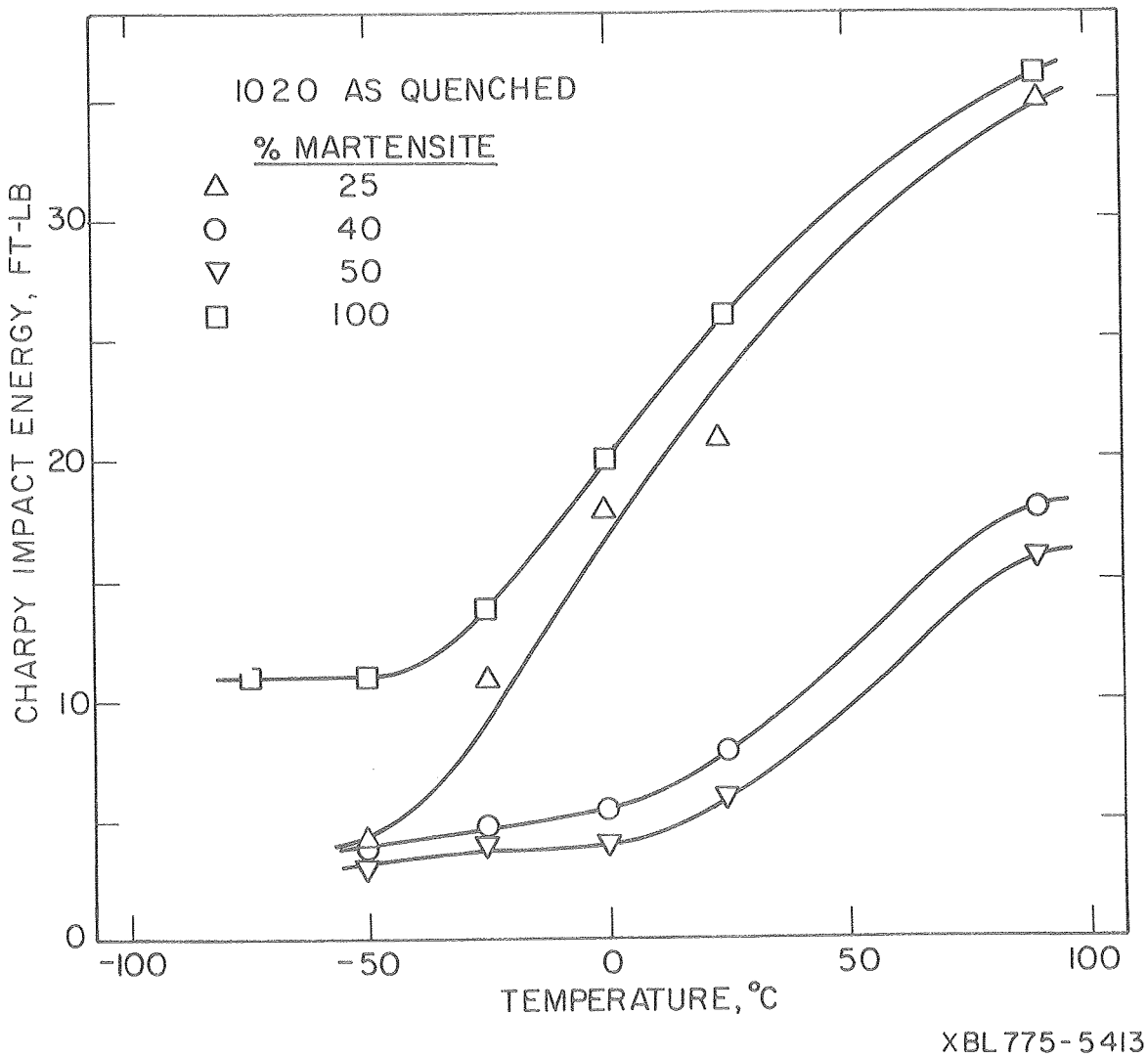
1020 AS QUENCHED
% MARTENSITE
25
40
50
100
CHARPY IMPACT ENERGY, FT-LB
0
10
20
30
-100
-50
0
50
100
TEMPERATURE, °C
XBL 775-5413

Fig. 20

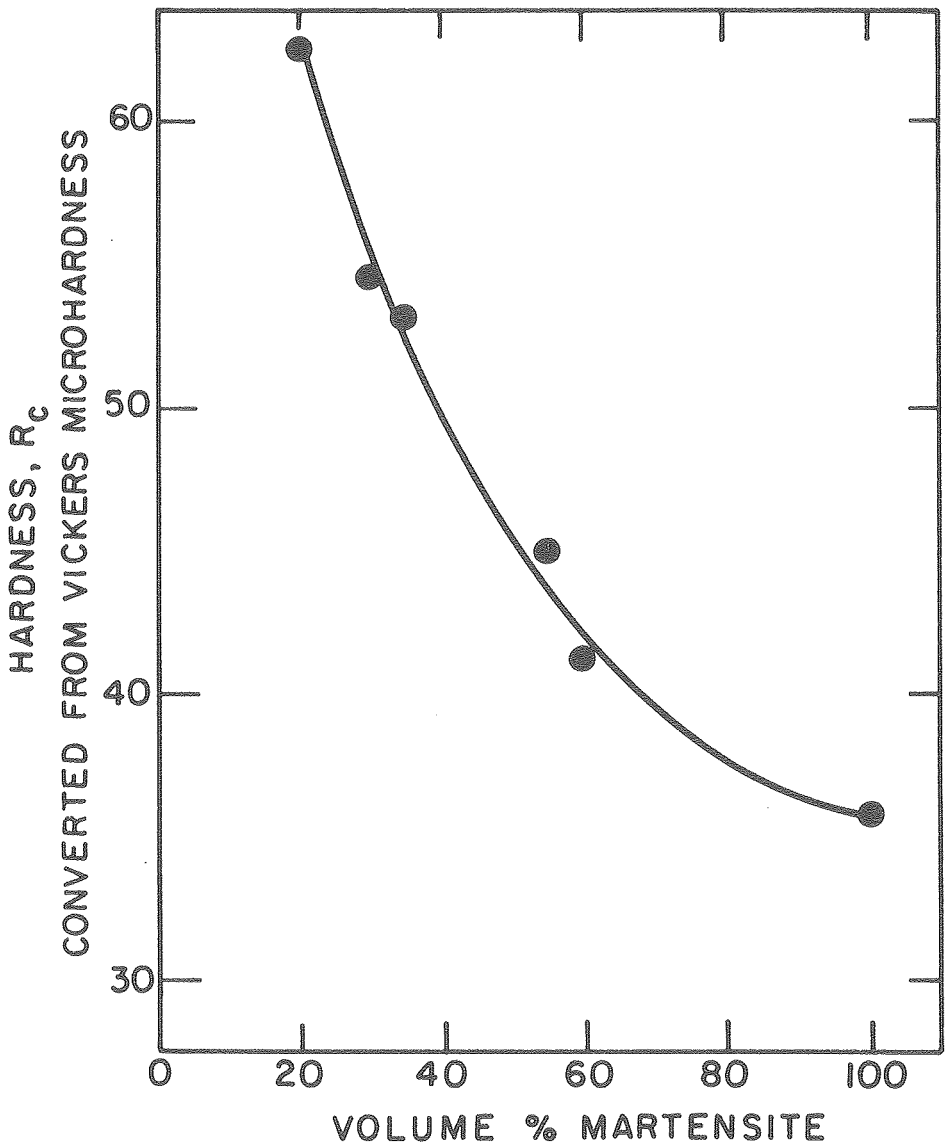

1010

Volume % Martensite	20	40	60	80
Approximate Carbon Content, Wt. %	0.45	0.25	0.15	0.12

XBL775-5405

Fig. 21

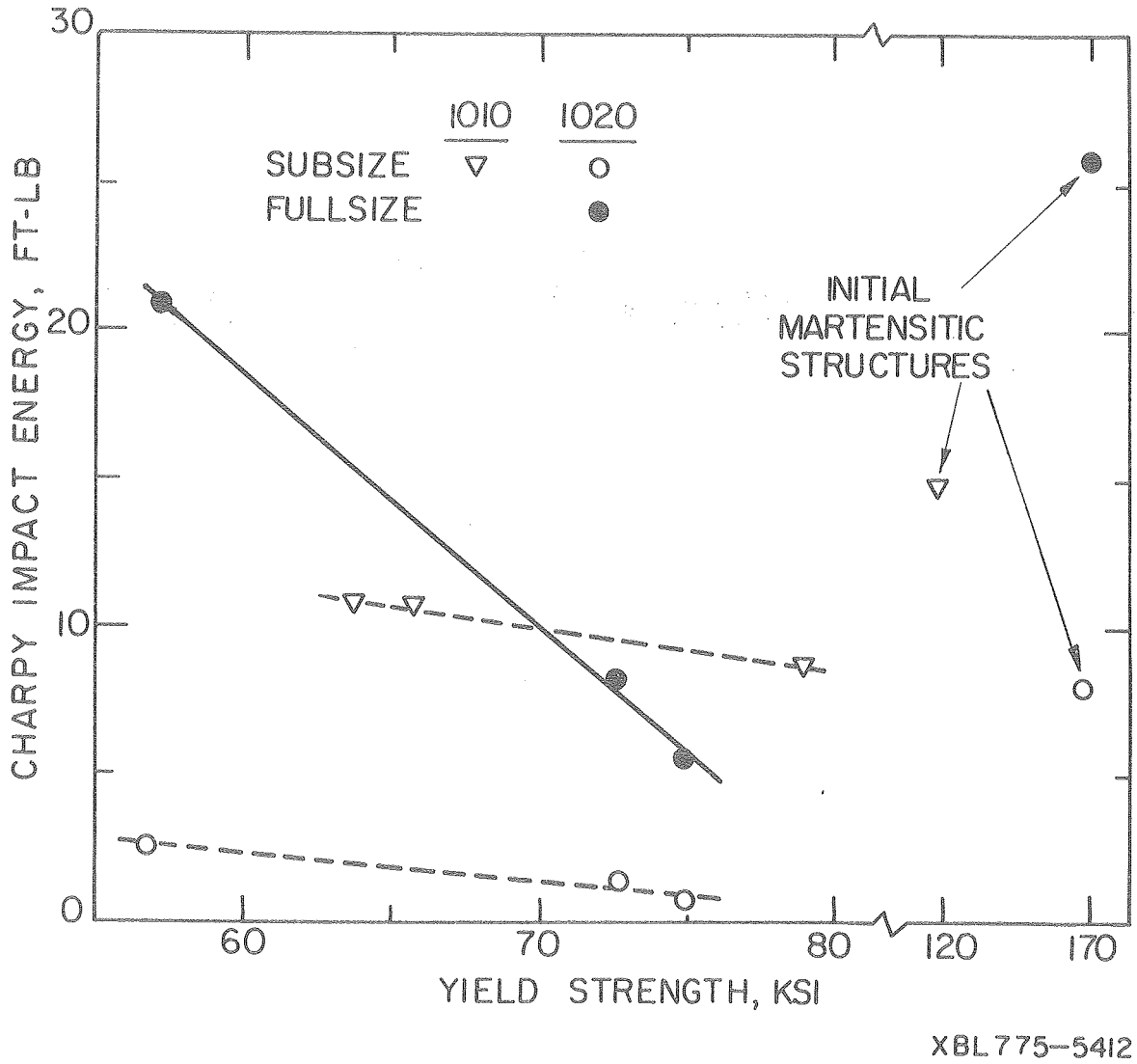
30
20
10
0
CHARPY IMPACT ENERGY, FT-LB
1010
1020
SUBSIZE
FULLSIZE
INITIAL
MARTENSITIC
STRUCTURES
60
70
80
120
170
YIELD STRENGTH, KSI
XBL775-5412

Fig. 22

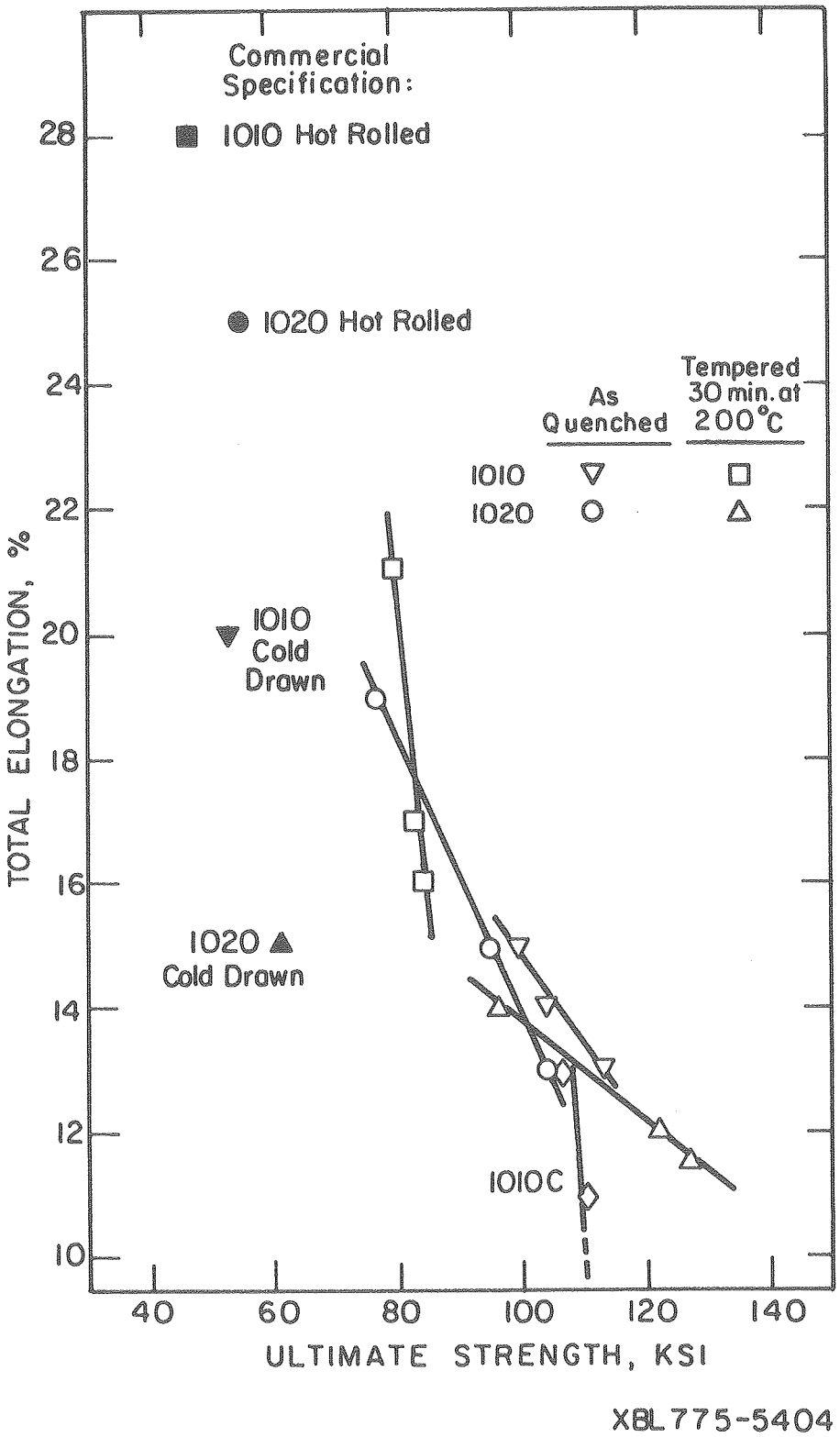
Commercial Specification:
1010 Hot Rolled
1020 Hot Rolled
As Quenched
Tempered 30 min. at 200°C
1010
1020
1010 Cold Drawn
1020 Cold Drawn
1010C
TOTAL ELONGATION, %
ULTIMATE STRENGTH, KSI
28
26
24
22
20
18
16
14
12
10
40
60
80
100
120
140
XBL775-5404

Fig. 23